T-3059

CHARACTERIZATION OF IN SITU HYDRATES AND THE EXPERIMENTAL MEASUREMENT OF THE RATE OF METHANE HYDRATE DISSOCIATION

by

Jeffrey W. Ullerich

ProQuest LLC.
789 East Eisenhower Parkway
P.O. Box 1346
Ann Arbor, MI 48106 – 1346

T-3059

A thesis submitted to the Faculty and the Board of Trustees of the Colorado School of Mines in partial fulfillment of the requirements for the degree of Master of Science (Chemical Engineering and Petroleum-Refining).

Golden, Colorado
Date 8/22/85

Signed: Jeffrey W. Ullerich
Jeffrey W. Ullerich

Approved: E. Dendy Sloan
E. Dendy Sloan
Thesis Co-Advisor

Approved: Sami Selim
M. Sami Selim
Thesis Co-Advisor

Golden, Colorado
Date 8/23/85

Arthur J. Kidnay
Professor and Head,
Chemical Engineering
and Petroleum Refining

Abstract

Naturally occurring hydrates recovered from site 570 of the Deep Sea Drilling Project were tested using bomb calorimetry. This test revealed that these hydrates contained more than the stoichiometric ratio of water. The samples tested ranged from 2-20 percent hydrate on a mass basis.

An apparatus to gather data on the dissociation of methane hydrates was constructed. This apparatus was checked and calibrated using ice and solid carbon dioxide. Methane hydrates were made in the laboratory for dissociation testing. Testing on these hydrates indicated a hydrate percentage of 70-90 percent. The data from methane hydrate dissociation was compared to the Selim-Sloan ablation model. The model underpredicted the data by 8-10 percent but predicted the trend of the data quite well.

Table of Contents

List of Figures

List of Tables

List of Illustrations

Acknowledgements

The author is grateful to the following persons and organizations for their intellectual and moral support during this study.

The Department of Energy for funding this research under Contract No. DE-AC21-83MC20693.

The Colorado School of Mines for providing financial support through the Colorado Fellowship.

Dr. E.D. Sloan for his instruction on hydrates and his encouragement.

Dr. M.S. Selim for many meaningful conversations and his confidence.

My parents for their patience and unceasing support and encouragement.

Nomenclature

A	=	Surface area of planar object
C_p	=	Heat capacity of hydrate
F	=	Thermal conductivity of hydrate
G	=	Gibbs free energy
H	=	Enthalpy
M	=	Mass of planar object
P	=	Pressure
S	=	Entropy
t	=	Time
t_{sd}	=	Start of dissociation time
T	=	Temperature
T_i	=	Initial temperature of hydrate
T_s	=	Equilibrium surface temperature of hydrate
V	=	Volume
X	=	Spatial position
$X^*(t)$	=	Dimensionless position of dissociation interface
Z	=	Compressibility factor
α	=	Thermal diffusivity of hydrate
$\delta(t)$	=	Thermal layer thickness
λ	=	Heat of dissociation of hydrate
ζ	=	Defined quantity (dimensionless)
θ	=	Defined quantity

ν = Stefan number (ratio of latent heat to sensible heat)

ρ = Density of hydrate

τ = Dimensionless time

τ_{sd} = Dimensionless start of dissociation time

Introduction

Naturally occurring gas hydrates may represent a large nonconventional source of energy. The existence of hydrates in permafrost environments, ocean and sub-ocean environments has been demonstrated (1). The question remains as to whether these hydrate deposits can be economically produced.

Understanding what to expect from hydrate deposits is a major concern. Until the recovery of naturally occurring hydrates at site 570 during the Deep Sea Drilling Project, no hydrates which existed in nature had been available for testing (2). This recovery afforded the possibility of study. As an initial study on these hydrates, work was done to determine the amount of gas contained in these recovered hydrates using bomb calorimetry.

A hydrate production model is necessary to economically produce hydrate deposits. A variety of production schemes has been suggested. These schemes employ the use of two basic approaches, thermal stimulation of the hydrate deposit and depressurization of the hydrate deposit. Much speculation has taken place; however, little experimental work has been done with hydrates in this regard.

As a fresh approach to the question of hydrate dissociation modelling, an ablation model has been proposed by Selim and Sloan (see Appendix A). This model incorporates the use of thermal properties of gas hydrates.

Experimental work on methane hydrates has been conducted to determine the applicability of this ablation model. Laboratory prepared hydrates were used in this investigation. Experimental work was conducted using an electrobalance and a vacuum system with a radiant heater providing the thermal energy of dissociation.

While naturally occuring hydrates contain a variety of gases, methane is the primary component. Therefore, methane hydrate dissociation data can shed light on the problems involved with the possible production of naturally occurring gas hydrate deposits.

Literature Survey

Inclusion Compounds

Inclusion compounds are physical combinations in which one component fits into a cavity in the other. A combination of considerable strength can occur when the shape and form of the guest molecule closely matches the cavity of the host molecule. No ordinary chemical bonding between the atoms of the host and guest are needed for stabilization. In stable inclusion compounds many atoms of the host molecule are in close proximity to the guest molecule and a sizable total bonding force is provided by the interactions of the outer electrons in the shells of the host and guest atoms. Such binding forces are known as dispersion forces.

Inclusion compounds are known to occur in six different forms depending on the molecular form of the host and the shapes of the cavities they enclose. Clathrates are produced when the guest molecules are enclosed in separate quasi spherical chambers within the crystal lattice. Canal complexes are formed when the host is a lattice having tubular cavities. Layer complexes are those

in which alternating layers of host and guest occur. Molecular sieves are formed by crystals that contain interconnecting chambers and passage ways. Interconnecting hollow space complexes are formed when the host molecule itself is large enough to have an internal cavity. The final form, linear polymer complexes, are found when guest molecules fit into the tube formed by a pipelike host molecule.

Many substances which are soluble in water contain water of crystallization when they crystalize out of solution. Called stoichiometric hydrates, most of these substances are not inclusion compounds but contain water molecules attached by the usual chemical bonds. The substances with which water does form true inclusion compounds are largely gases or low-boiling-point liquids. These complexes are known as gas hydrates and fall into the clathrate form of inclusion compounds. Following his work with inclusion compounds between 1947 and 1950, H. M. Powell of the University of Oxford suggested the appropriate term clathrate (3). The origin of this term is the Latin word clathratus, which means enclosed by the bars of a grating.

Hydrate Structure

X-Ray crystallographic studies by M. von Stackelberg and his coworkers at the University of Bonn(4), by Walter F. Claussen at the University of Illinois (5) and by Linus Pauling and Richard E. Marsh (6) at the California Institute of Technology have shown that the water molecules in these clathrates are linked together through hydrogen bonds. A ring structure of five water molecules is formed rather than the six molecule rings typical of ice. These five member rings join together to form dodecahedrons (12 sided figures). Since no arrangement of dodecahedrons can completely fill a space, some interstitial spaces remain. It is in these interstitial spaces found in the dodecahedrons, that the guest molecules are found.

Gas hydrates may take two different structural forms. The unit crystal of Structure I (body centered cubic) and the unit crystal of Structure II (diamond lattice) are shown in Figure 1. Each hydrate structure has two types of quasi-spherical cavities of differing diameter. The properties of the gas hydrate lattices are shown in Table 1 (1).

The unit cell of Structure I is constructed of 46

Figure 1

Hydrate Stucture

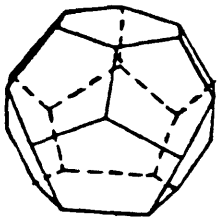

Tetrakiadecahedron

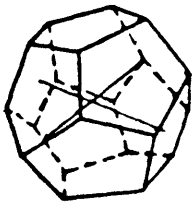

Dodecahedreon

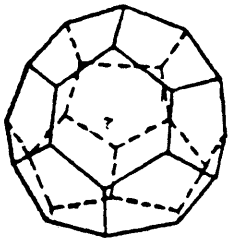

Hexakaidecahedron

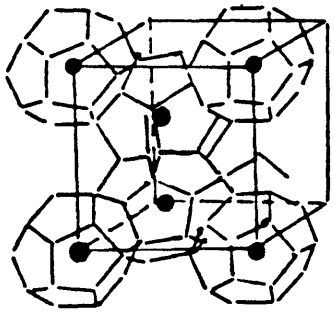

Structure I

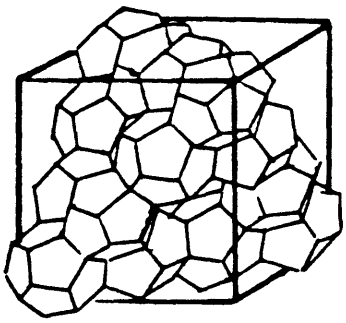

Structure II

TABLE 1

Properties of Hydrate Structures I and II

Property	Structure I	Structure II
Unit Cell Size (angstrom)	12.03	17.31
Number of Dodecahedra	2	16
Number of Tetreakaidecahedra	6	0
Number of Hexakaidecahedra	0	8
Water Molecules / Unit Cell	46	136
Cavities (cages) / Unit Cell		
Small	2	16
Large	6	8
Cavity Radius (angstrom)		
Small	3.94	3.91
Large	4.30	4.73

water molecules forming eight cavities for gas molecules to occupy, consisting of two smaller and six larger cavities. A pentagonal dodecahedron arrangement forms the smaller cavities. The larger cavities are tetrakaidecahedron formed by two opposing hexagons and twelve accompanying pentagons situated between. When all eight cavities are occupied, a ratio of 5.75 water molecules per gas molecule is obtained.

In Structure II, 136 water molecules form a lattice containing eight larger and sixteen smaller cavities. At total filling a ratio of 5.67 water molecules per gas molecule is obtained. The smaller of these cavities is a somewhat deformed pentagonal dodecahedron. The large cavities of Structure II are hexakaidecahedron, each consisting of four hexagons and twelve pentagons.

The type of structure formed depends on the geometry of the gas molecule. In general, small gas molecules form Structure I hydrates, while larger gas molecules form Structure II because of its larger cavities. Two factors are important in determining if a gas will hydrate. These factors are molecular length and the physical configuration of the molecule. Several molecules are non hydrate-formers, even though molecules of greater length may form hydrates. Structure II is inherently more stable

than Structure I, due to the approximately tetrahedral angles found in Structure II hydrates. This stability of Structure II hydrates allows them to exist in a wider range of natural environments.

Hydrate Occurrence and Resource Potential

Natural gas can combine with water to form solid hydrates in areas of high pressure and low temperature. These conditions exist onshore in sediments in and beneath thick permafrost and offshore beneath water deeper than 1500 feet. In order to form hydrates an available source of hydrocarbons must also be present.

Onshore hydrates occur in and under permafrost regions. Permafrost, or perennially frozen ground, is naturally occurring material which has remained colder than $0^{0}C$ continuously for two or more years. Permafrost covers more than 23 percent of the earth's land area. This land is found in Alaska (75 percent of total area), Canada (63 percent), the USSR (47 percent), the polar regions of Scandinavia, Greenland, and Antarctica.

Since hydrates of natural gas may occur in sediments beneath the world's oceans where the water depth is greater than 1500 feet, the area available for potential offshore

hydrates is 3.0 X 10^8 km^2, more than 90 percent of the ocean basins. The temperature of ocean water decreases with depth, with the bottom temperature in the open ocean generally in the range from 30^o to 35^o F. This fact increases the vertical extent to which hydrates may be stable. However, once the water and sediment interface is reached normal geothermal temperature gradients are encountered, which means temperature increases with depth.

Since such a large area of the earth can potentially contain hydrates, the volumes of gas bound in hydrates may be enormous. The largest estimate (by Dobrynin) indicates that up to 3 X 10^8 trillion cubic feet (TCF) of natural gas may exist in hydrate form. Gas hydrate resource estimates are shown in Table 2 (1). The estimates vary widely because of the scarcity of available data.

Dobrynins' estimate is quite optimistic, assuming hydrates exist in all possible areas, while Meyers' estimate is based on a literature review of identified occurrences and a subjective interpretation of this data.

Hydrate Research History

Knowledge and interest in gas hydrates have gone through four phases. In 1810 Sir Humphrey Davy (7) bubbled

Table 2

Gas Hydrates Resource Estimates, TCF

	Onshore		Offshore	
	World	USA	World	USA
Dobrynin, 1979	$1.2X10^6$	25,000	2.710^8	$6.7X10^6$
McIver, 1979	1,100	23	$1.1X10^5$	2,700
Meyer, 1979	500	11		
Trofimuk, 1980	2,010	42	$2-9X10^5$	4-21,000

chlorine gas through water under atmospheric conditions at temperatures near the freezing point of water. A yellow precipitate resulted, which Davy named chlorine hydrate. This hydrate was analyzed by Faraday in 1823 (8). It was not until the 1890's that French scientists made significant studies on which gases form hydrates. Significant data on formation conditions was gathered, but it was not until the 1950's that the structure was known (5,9).

The petroleum industry initiated the second phase of hydrate research. For many years it was assumed that ice plugged natural gas pipelines until in the 1930's when Hammerschmidt (10) showed hydrates to be the cause. He also showed that hydrates could form at temperatures well above the freezing point of water and that additives (e.g. methanol) inhibit the formation of hydrates.

The third stage began in the 1950's when von Stackleberg (4) and coworkers used X-ray diffraction to determine the crystalline structure of hydrates. The way was now open for the development of theoretical models by van der Waals and Platteeuw (11).

In the late 1960's natural gas hydrates were discovered in nature and the fourth stage of hydrate research had begun (12). This development was followed by

theoretical studies and confirming indications of hydrates from wells in Alaska, Canada, Siberia, and offshore areas. With these dicoveries excitement was generated that hydrates could be a large, naturally occurring gas resource.

Recovery of Natural Hydrates

On leg 84 of the Deep Sea Drilling Project naturally occurring samples of ocean bottom hydrates were recovered for onshore testing (2). On this leg gas hydrates were observed at three locations (565, 568, and 570). A core of gas hydrates was recovered from site 570 (latitude, 13^{0} 17.1′ N; longitude, 91^{0} 23.6′ W). This core was obtained in upper slope sediment at a depth of 1718 meters. The hydrate core measured 1.05 meters in length and 5.6 centimeters in diameter. Electric logging of the borehole conducted later revealed that this core came from a seam of hydrate 3 to 4 meters in thickness. This core sample is the first massive gas hydrate ever to be recovered from oceanic sediment, and it is the first sample of marine gas hydrate to be preserved for onshore testing.

In anticipation of such a discovery, four hydrate

sample containers were fabricated at the Colorado School of Mines. These sample containers were made from Air Force 304 stainless steel oxygen cylinders. Each cylinder was fitted with a high pressure flange, hydrostatically tested, and placed on shipboard prior to sailing.

Samples from the recovered core were placed in prechilled cylinders and stored in a freezer at 263 K. After the drilling ship returned to port, the cylinders were transported overland from San Diego to the Colorado School of Mines in Golden, Colorado. The cylinders were packed in dry ice during the journey. A visual leak inspection was conducted after the samples and cylinders reached the laboratory. This inspection was conducted by immersing the cylinders in an aqueous solution of ethylene glycol at 253 K. After passing the leak inspection, the cylinders were placed in a freezer maintained at 230 K. Portions of the sample were subsequently distributed to eight investigators.

Tests On In Situ Samples

The recovery of the offshore hydrates afforded the first opportunity for detailed experimental analysis in shore based laboratories. Such analysis was aimed at

identifying the extent of the resource and determining methods of producing gas from hydrates. With these two goals in mind, the measurement of important physical properties was undertaken (2).

After recovery and transport to the laboratory at the Colorado School of Mines the sample was distributed to several researchers. These researchers came from private industry, government agencies and the academic community. This disbursement was made with the understanding that each researcher would address the measurement of certain properties and share any information. Table 3 details the experiments undertaken and the responsible investigator.

Following the completion of the work by K. A. Kvenvolden and G. E. Claypool of the United states Geological Survey (13), questions were raised concerning the hydrate samples. Particular concern was directed toward the gas content of the samples. It was found in their studies that more than the stochiometric ratio of water to gas was obtained on dissociation. The observed ratio was one molecule of methane to every nineteen to twenty molecules of water, which was in contrast with the stochiometric ratio of 1:5.75. Therefore, in addition to the work to be conducted at the Colorado School of Mines, further studies were proposed to address this question.

Table 3

Shore Based Experiments on Site 570 Hydrates

Institution	Investigator	Measurements
Colorado School of Mines	E.D. Sloan	1. Heat Capacity 2. Heat of Dissociation 3. Dissociation Rate 4. Thermal Conductivity
Department of Energy (METC)	R.D. Malone	1. Accoustic Velocity 2. Electrical Resistivity
National Bureau of Standards (Boulder)	J.E. Callanan	1. Heat Capacity 2. Thermal Conductivity 3. Thermal Expansion 4. Heat Flow Studies 5. Fracture Resistance 6. Hardness 7. Elastic Wave Velocity

Standard Oil of Ohio	R.L. Horton	1. Pulsed NMR Spectroscopy 2. Mechanical Properties 3. Focussed Acoustic Attenuation 4. Broad-Band Microwave Attenuation
Texas A & M University	J.M. Brooks	Carbon isotopes for: methane ethane carbon dioxide
University of California	B. Barraclough	1. Deuterium analysis 2. Oxygen Isotopic Analysis 3. Chlorinity
United States Geological Survey	K.A.Kvenvolden G.E. Claypool	1. Gas Composition 2. Water/Methane Ratio 3. Pressure Changes on Gas decomposition

The method of bomb calorimetry was used to determine the portion of the sample which was hydrate and that work comprises a portion of this thesis work.

Bomb Calorimetry

Early literature reports observations made with combustion calorimetry and the data from the later portion of the eighteenth century (14). In 1784, Lavoisier and La Place described an ice calorimeter from which heats of combustion were determined. Davy in 1817 reported results of combustion studies in which gases were burned in air and oxygen. In 1848, Andrews determined the heats of combustion of a variety of substances, such as methane, ethane, hydrogen, carbon dioxide, sulfur, phosphorous, carbon and many metals. The substances were burned in what is believed to be the first bomb calorimeter.

Bomb calorimetry is an important method of determining the heats of combustion of a wide variety of compounds. Gases, liquids, and solids can all be combusted in such an apparatus. This method of experiment has been popular since the late eighteenth century, with many notable scientists contributing to its advancement.

Modeling Hydrate Dissociation

Since hydrates have been postulated to be a major potential energy resource, considerable effort has been devoted to the modeling of hydrate dissociation. This modeling work has been in preparation for developing viable production schemes for the future. These models have ranged from the mathematically simple to the mathematically complex. In all cases important physical data on hydrates is needed, namely the heat of dissociation, the heat capacity, and the thermal conductivity.

Hydrate dissociation energy is defined as the energy required to create a phase change and thus dissociate hydrate into its components, gas and water or ice. Deaton and Frost (15) detailed a method to calculate the dissociation energy or the enthalpy of formation using the Clapeyron equation. The necessary data to make this calculation on methane, ethane, propane, and natural gas hydrates accompanies this development.

Some experimental work has been done to determine the heat of dissociation. During the last century, Villard (16) measured the heats of dissociation of CO_2 and N_2O hydrates, obtaining a value of 63 KJ/mole. Nagayev (17)

calorimetrically measured the heats of dissociation of CO_2 hydrate and found that it decreased from 57.98 KJ/mole at 281 K to 53.1 KJ/mole at 279 K. Recently, Cherskii. et al (18) made measurements on prepared natural gas hydrates. These laboratory prepared hydrates were formed so as to be typical of those found in most gas fields in the USSR. Cherskiis' study indicated that the heat of dissociation of natural gas hydrate ranges from 520 to 540 kJ/mole.

Heat capacities as a function of temperature for tetrohydrofuran (THF) II, ethylene oxide (EtO), and cyclopropane have been reported by Callanan and Sloan (19). Heat capacity was found to vary both with structure and with guest molecule. Cherskii et al (20) has made some measurements of the heat capacity of natural gas hydrates. The results of this work in equation form is: $C_p = 2.16 + 8X10^{-3}T$. Temperature is in degrees Kelvin and the heat capacity value has units of kJ/kg/K.

Few measurements have been made on the thermal conductivity of natural gas hydrates. Stoll and Bryan (21) have reported an approximate value of $0.94X10^{-3}$ cal/cm/sec/K. This value is suprisingly low, only about one-fifth that of ice and the reason for this difference is not clear. Dharmawardhana (1) has suggested that the difference may be due to streching of the angles normally

found in ice. Ross and Andersson (1), as well as other investigators, believe a phonon scattering mechanism is involved.

Two different approaches have been suggested for the exploiting of hydrate reserves. These two approaches are thermal recovery and depressurization. Thermal recovery of a hydrate reservoir involves injecting energy to first heat the reservoir matrix and its associated fluids to the dissociation temperature and then adding additional energy to dissociate the hydrate. Depressurization of a hydrate reservoir results in the dissociation of gas hydrates when the pressure is lowered until the phase boundary is crossed. Depressurization results in the cooling of the unproduced section of the reservoir.

Each of these methods has its proponents, and each approach has been considered in its simple and complex forms. A comparative review of American and Russian models indicates that the Russian models have reached a greater level of mathematical sophistication because the Russians have been aware of hydrates in their reservoirs almost a decade longer.

Holder, et al (22) conducted a thermodynamic evaluation of hydrate production. This thermal recovery model evaluated only the potential of hydrate production

from a thermodynamic viewpoint and found it viable. However, this model relies on a completely general thermodynamic analysis which delineates the significance of various geophysical parameters.

Various other thermal stimualation models have been proposed. A production scheme for deep water hydrate deposits suggested by Rose and Plannkuch (23) envisions the use of deeply buried geopressured-geothermal aquifer water, or other warm ocean surface layer water. Circulation under the hydrate layer would provide the energy necessary for partial decomposition. While this idea is very speculative and no actual mathematical modeling is done, the work does stress that it is time to address the question of recovery of natural gas from hydrate deposits. Another hot brine technique has been proposed by Kamath and Godbole (24). In this work a mathematical model is developed to compute gas recovery and energy efficiency ratio for a reservoir containing a single zone of gas hydrates trapped between impermeable rocks. This model exhibits some complexity as evidenced by the fact that wellbore heat losses and heat losses to overburden and underburden formations were included in the overall energy balance calculations. This theoretical study reaches the conclusion that there is a good potential for the brine injection technique.

McGuire (25) also postulated a hot water flooding technique. The method for which equations are developed involves forcing hot water down an injection well and producing from another. After various mathematical calculations, the conclusion is reached that the hydrates may be a viable resource but that many numerous important questions need to be answered.

Cherskii and Bondarev (26) have proposed a thermal model for producing gas hydrate deposits. The developed mathematical model is a variation of the Stefan problem, because the temperature on the moving boundary is a function of pressure. The equations are solved analytically, but no computational work accompanies the solution.

Thermal recovery techniques may be problematic in the severe environments where hydrate fields are likely to exist. While the energy required to dissociate the hydrate represents only ten percent of its heating value, heat losses to the surroundings may be quite large. Therefore, depressurization techniques have also been investigated.

Holder (27) has suggested using a recovery method involving the sensible heat of the hydrate reservoir to provide the energy necessary for hydrate dissociation. Appropriate modeling equations are developed and solved by

a finite difference technique. Results clearly indicate that hydrates adjacent to a conventional gas reservoir may contribute significantly to its gas production.

Russian investigators have also developed models for pressure reduction decomposition of hydrates. Verigin, Khabibullin, and Khalikov (28) proposed a model for the dissociation of gas in a porous medium. Appropriate solutions are obtained for the linearized equations of the flow of a gas in porous regions with a moving interface that describe the dissociation of gas hydrate when the pressure is reduced. Calculations are made to predict the position of the hydrate dissociation front and the instantaneous gas flow rates at different times.

A New Ablation Model

A more fundamental approach to modeling hydrate dissociation has been made by Selim and Sloan (29). Fundamental physical and mathematical principles are considered in developing this heat transfer controlled model. The model assumes dissociation of a pure hydrate using a constant heat flux incident on a planar semi-infinite medium with constant physical properties. The water formed during the dissociation process is assumed

to be blown away by the gas so that the dissociation process may be regarded as a moving-boundary ablation problem. The governing differential equations describing the dissociation are presented and a solution is obtained using the Von Karman integral method.

The solution of this problem in dimensionless terms is given by:

$$X^* = (1-\zeta) + \nu \ln\left(\frac{\nu}{(1+\nu)-\zeta}\right)$$

and:

$$\tau-\tau_{sd} = (1-\zeta) + (1+\nu)\ln\left(\frac{\nu}{(1+\nu)-\zeta}\right)$$

In these equations X^* is dimensionless distance of the hydrate front, τ is dimensionless time, ν is the Stefan number, and ζ is a defined dimensionless quantity. The appropriate equations to define the position of the moving front with time are:

$$X = 4k(T_s-T_i)X^* / (5F)$$

and:

$$t = 4\rho\lambda k(T_s-T_i)\tau / (5F^2)$$

The solution to this problem in dimensionless terms, for various values of the Stefan number ν is presented in Figures 2 and 3. Results from these figures can, therefore, be used directly to determine the amount of

hydrate dissociated as a function of time. These figures lead to the development of a long time solution. It was noticed that the speed of the interface decreases with time; eventually attaining a constant value. The long time solution obtained is:

$$X^* = \frac{\alpha F/k(T_s - T_i)}{1+\nu} \qquad \text{for large } t$$

For a detailed development of the model see Appendix A.

Figure 2

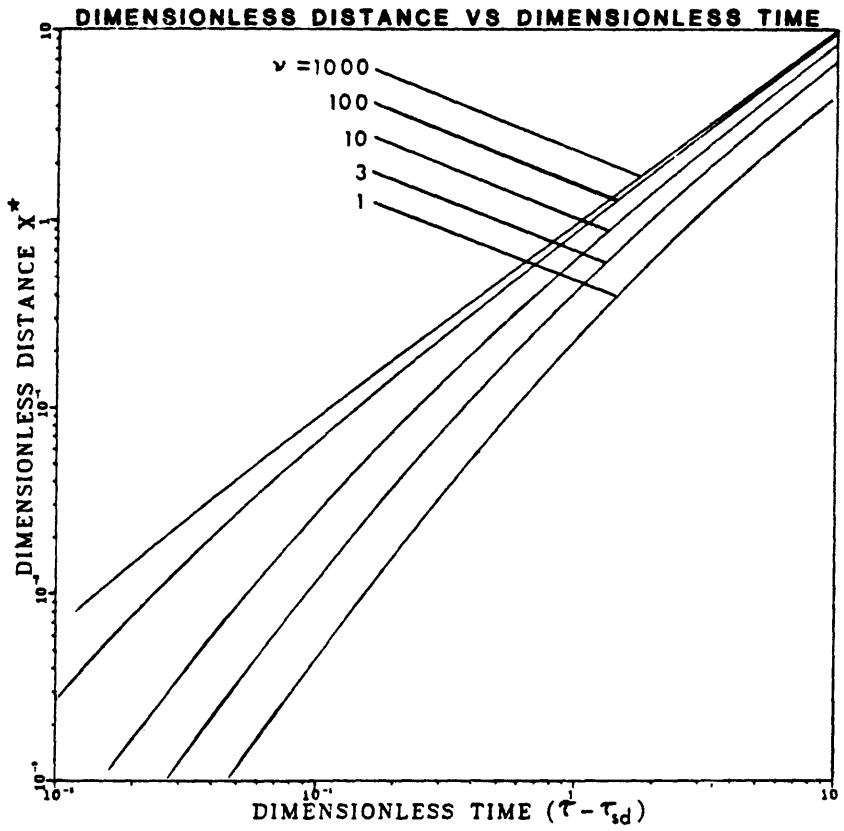
DIMENSIONLESS DISTANCE VS DIMENSIONLESS TIME
ν =1000
100
10
3
1
DIMENSIONLESS DISTANCE X*
DIMENSIONLESS TIME (τ - τsd)

Figure 3

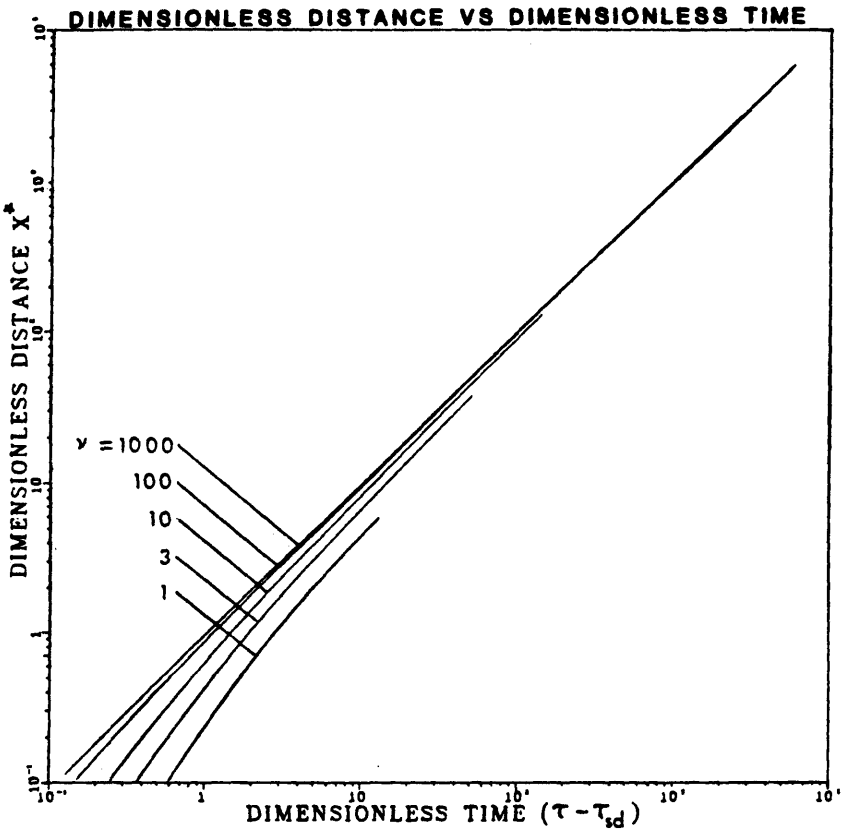
DIMENSIONLESS DISTANCE VS DIMENSIONLESS TIME
DIMENSIONLESS DISTANCE X^*
DIMENSIONLESS TIME $(\tau - \tau_{sd})$
ν = 1000
100
10
3
1

Experimental Equipment

The data collected in this experimental investigation was produced using three separate apparatus. Data taken to determine the per cent hydrate in the insitu samples was obtained using a bomb calorimetry apparatus. Dissociation experiments were conducted by utilizing a Cahn electrobalance in a vacuum system. Hydrates needed for the dissociation experiments were made in the lab using a cooling bath and stainless steel formation vessel. All three pieces of apparatus are described in detail below with accompanying figures.

Bomb Calorimetry

The Parr calorimeter, model 1341 used in these experiments is an improved version of the bomb calorimeter which has been manufactured by Parr for more than sixty years and is shown in Figure 4 (30). Although commonly called a 'plain' calorimeter because of its simple design, technically, this is a static jacket instrument which operates at or near room temperature with no provision for temperature adjustment or control. Correction for any heat

Figure 4

Calorimeter Cross Section

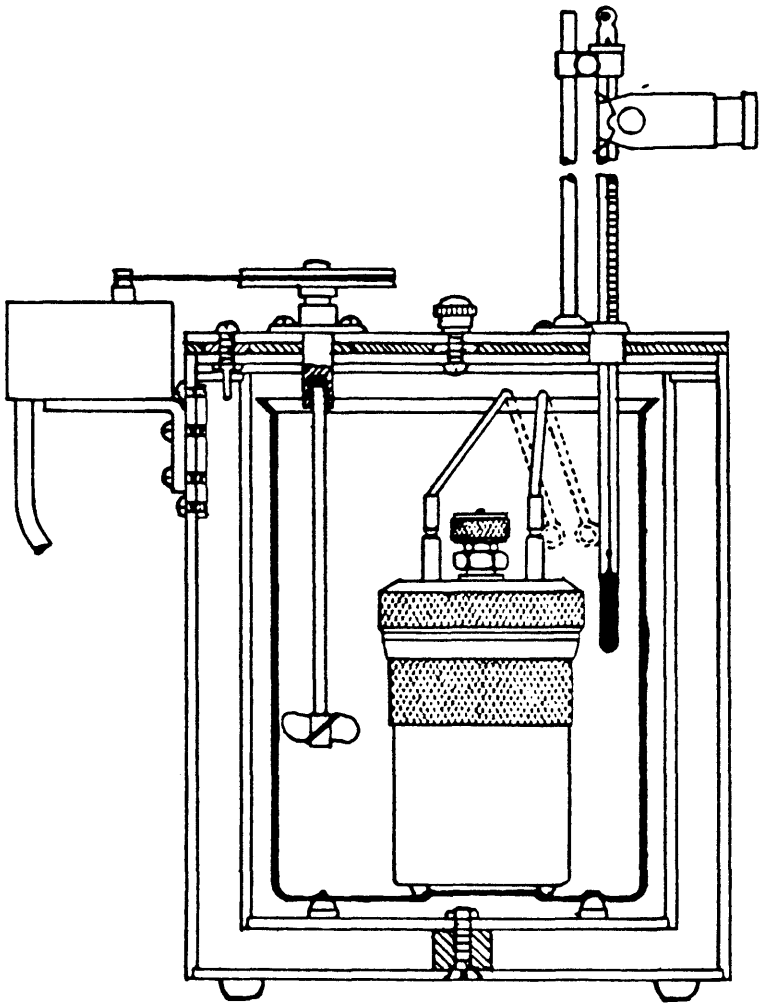

loss (or gain) during an experiment is made by applying a correction calculated from the heat leak measurements taken immediately before and after each test. When operated with care the precision obtainable with this calorimeter will approach that expected from most general purpose adiabatic calorimeters.

The most important component of the calorimeter is the combustion bomb itself (see Figure 5). Made from 29 Ni, 20 Cr stainless steel the combustion bomb has an internal volume of 342 ml. The bomb head is equipped with two valves. On the inlet side there is a check valve which opens when pressure is applied and closes automatically when the supply is shut off. On the outlet side the gases are released through a needle valve. A tank of oxygen with a purity of 99.5 per cent is used to supply the necessary oxygen to insure complete combustion. The bomb head is also equipped with two banana jack connections. These connections are used to ignite the sample. An ignition unit which operates from a standard electrical outlet provides the proper voltage firing current. The ignition circuit is completed by connecting the two electrodes with a nickel alloy fuse wire with a heat of combustion of 2.3 cal/cm. All solid samples placed in the accompanying sample basket are in good contact with the fuse wire and

Figure 5

Cross Section of Combustion Bomb

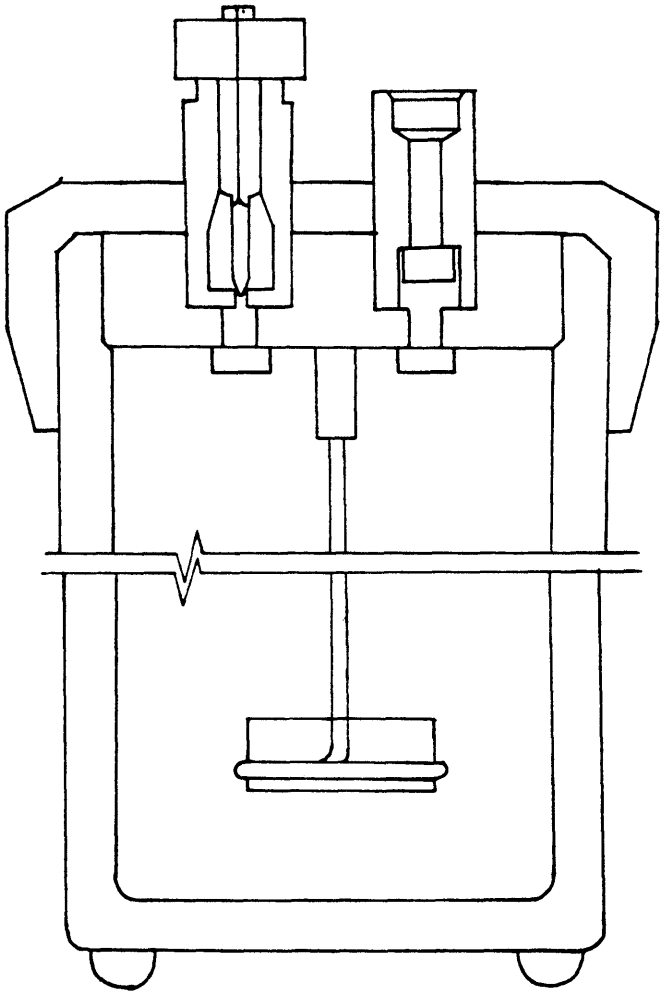

have been pressed into pellet form using a pellet press. Pellets are easier to handle than loose samples and burn more slowly in an oxygen bomb, thereby insuring more complete combustion.

Temperature measurments are one of the important pieces of data taken during each test. These measurements are taken by monitoring the temperature increase in a known mass of deionized water. The thermometer used in this case is accurate to 0.005 ^{0}C and the mass of the deionized water is determined on a balance with a 0.1 gram sensitivity. Good mixing is maintained in the water through the use of a mechanical stirrer.

Benzoic acid was used to standardize the bomb calorimeter. The term standardization here denotes the operation of the calorimeter on a standard sample from which the energy equivalent or effective heat capacity of the system can be determined. The energy equivalent is the energy required to raise the temperature one degree, expressed as calories per degree Celcius. At the first International Conference on Chemistry of the International Union of Pure and Applied Chemistry (IUPAC) held in Rome in 1920, it was proposed that a thermochemical standard for the heats of combustion of organic compounds and fuels be adopted (14). A commission was nominated to study the

problem. In 1921, in Brussels at the second International Conference of Chemistry of the IUPAC, a resolution was adopted in which benzoic acid was formally adopted as the thermochemical standard for the bomb calorimeter.

Two other pieces of equipment were used in conjunction with the bomb calorimeter. The first is a Sako balance accurate to one milligram which was used to determine the sample masses of the insitu hydrates. Secondly, gases were analyzed by gas chromotography. The chromatograph manufactured by Carle is a Series S Model 111H and works on the principle of thermal conductivity. The following gases are detectable.

hydrogen	isobutylene
propane	trans-butene-2
propyene	cis-butene-2
isobutane	1,3 butadiene
hydrogen sulfide	isopentane
n-butane	butene
n-pentane	ethylene
carbon dioxide	ethane
oxygen	nitrogen
methane	carbon monoxide
C_5^- and $C_5^{=+}$	

Disssociation

The apparatus for the dissociation or sublimation experiments is an assemblage of equipment (see Figure 6). The primary component is a Cahn 2000 recording electrobalance equipped with a vacuum bottle. This balance is capable of making both static and dynamic weight measurements with a precision of ± 1.0 microgram, when properly calibrated. Equipped with two mass determining positions the balance can be used in a variety of applications. When using the A loop (see Figure 7) a mass of one gram can be measured with an accompanying mass loss of one hundred milligrams. Loop B on the other hand allows mass determinations on samples of up to two and one half grams with an accompanying mass loss of one gram.

The Cahn 2000 balance may be best described as an electric current to torque transducer. The balance beam pivots without the use of a knife edge or jewel pivots but instead uses a taut band suspension, which results in a more reliable balance that provides accurate and reproducible weighings. The balance beam is mounted to, supported by, and pivots about the center of this taut ribbon. The Cahn 2000 is equipped with a photo cell which

Figure 6

Listing of Equipment

1. Electrobalance and vacuum bottle
2. Electronic controls for electrobalance
3. Strip chart recorder
4. Heater
5. Variable voltage supply
6. Barocell
7. Electronic Manometer
8. Diffusion pump
9. Vacuum pump
10. Vent

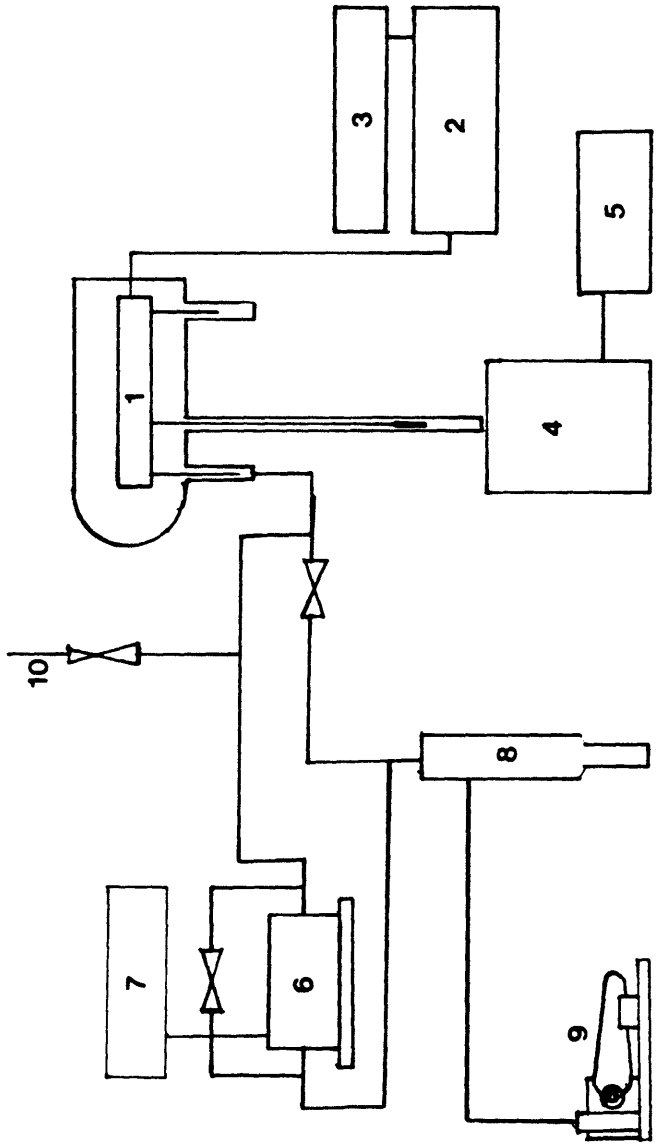

Figure 6
Dissociation Apparatus

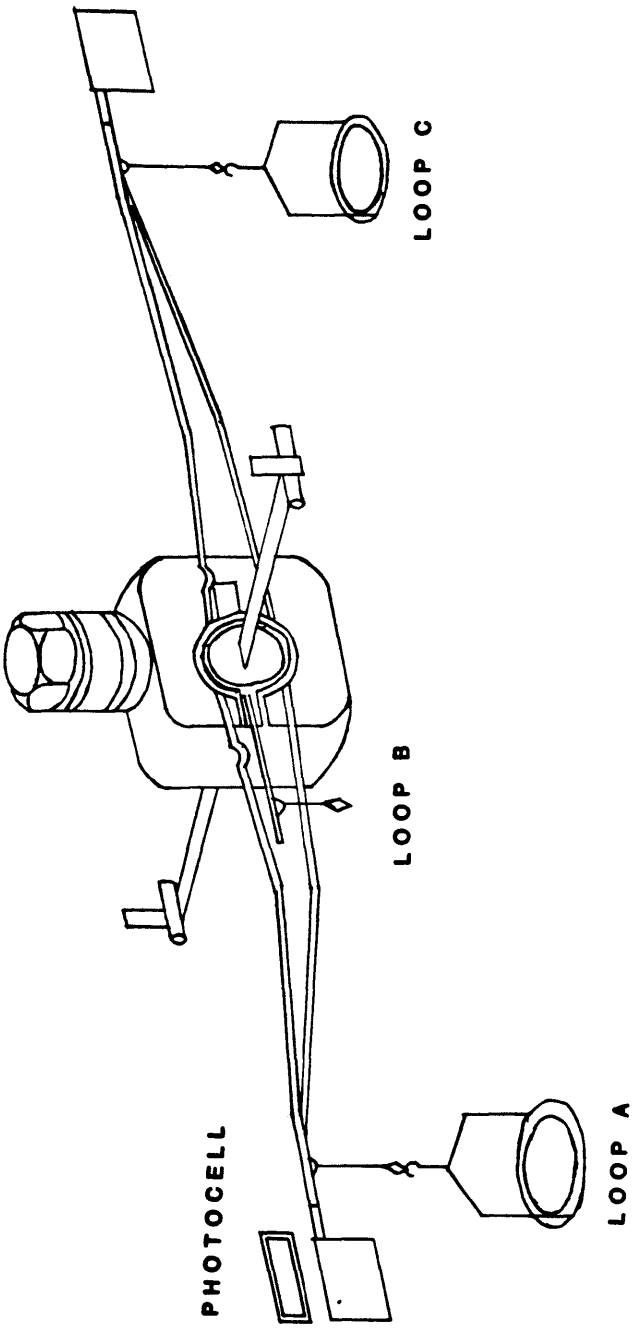

Figure 7
Electrobalance

senses an unbalanced condition. To restore a balanced condition an appropriate amount of torque is applied to the gold plated balancing mechanism by the torque motor coil which is located in a permanant magnetic field and mounted to the taut ribbon. All electronics are external to the weighing compartment allowing use in vacuum applications.

The electronic signal processing equipment allows the user of the balance to complete several useful functions. Among these functions are two which are of primary importance, namely, signal zeroing and balance calibration. The calibration function is accomplished by using a class M calibrating weight. The recorder range can also be adjusted to observe smaller weight losses with time. Equipment is also available to supress a portion of the output signal from the electronics. The signal suppression is in porportion to the mass suppressed. Mass suppression is accomplished by digital thumbwheel switches. A three position electronic filter reduces signal noise due to most external vibrations.

The electronic signal is sent to a Houston Instruments Omniscribe model B-5000 strip chart recorder, which is a two channel, high impedence recorder (Z= 100 Mohm).

The other major piece of equipment is a barocel and electronic manometer combination manufactured by

Datametrics. The model 570D Barocel is a differential pressure sensing capacitive potentiometer arranged in a bridge circuit such that the diaphragm motion changes the capacitance. Changes in capacitance are then electronically manipulated by the model 1174 electronic manometer into pressure indications. The pressure is displayed on a digital readout. Pressures in the range from 0.0 - 1000.0 Torr may be determmined with this barocel.

Energy is supplied to the sample from a radiant heater (see Figure 8). This heater consists of a 1.5 inch inside diameter Quartz tube with a 2.0 inch outside diameter, wrapped with a coil heating element. Coiling of the heating element eliminates inductance during power consumption, therefore the power equation for direct current is applicable even though alternating current is used. The amount of voltage applied to the heater is regulated using a variable voltage supply. Both the current and voltage across the heating coil can be measured. The outside of the heater is wrapped with three layers of Kaowool insulating blanket. Marinite caps are secured to both ends of the heater. A type J themocouple in good thermal contact with the outside of the quartz tube is used to measure the temperature of the radiating quartz

Figure 8

Heater Cross Section

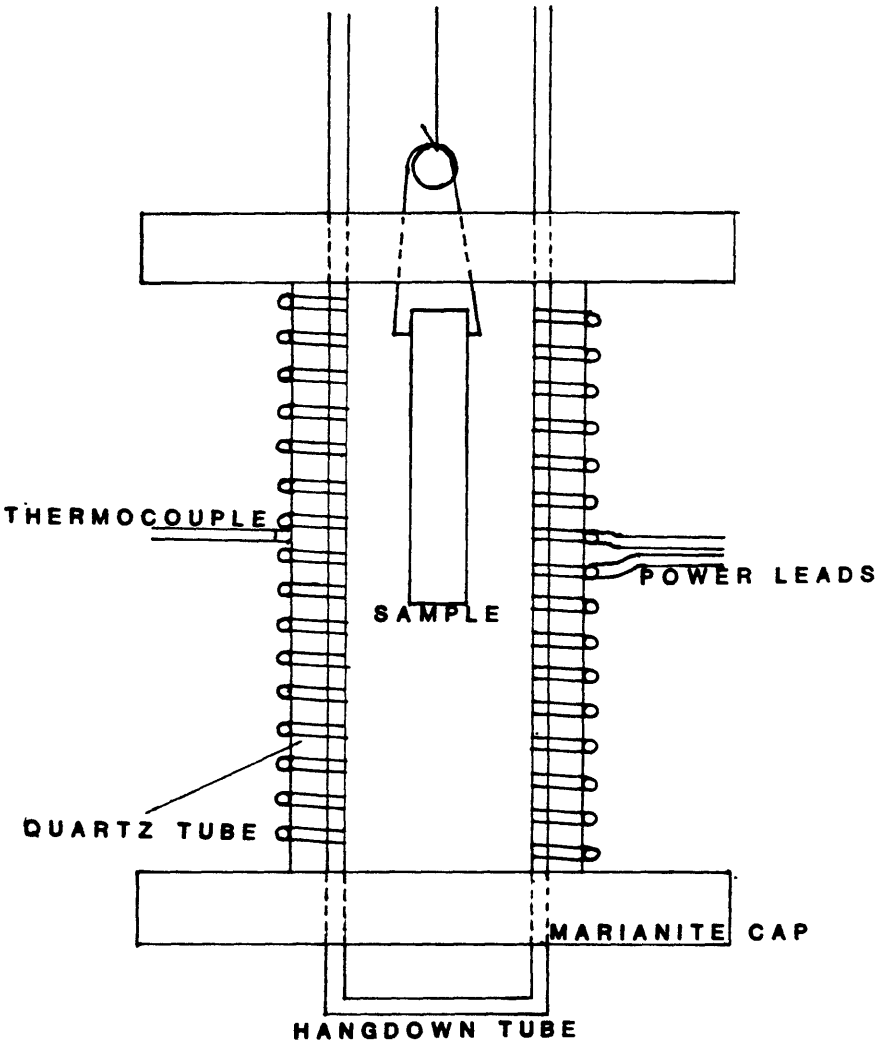

surface. To minimize heat loss from the outside of the heater additional insulation surrounds the heater. Two one inch thick layers of a six pound per cubic foot density Fiberfrax Durablanket insulation manufactured by Carborundum are used. Both the heater and this added insulation, which surrounds the heater on all sides, have been sealed in a box constructed from composition board.

A Pyrex hangdown tube surrounds the sample during the experiment. This hangdown tube is in direct contact with the quartz tube inside the radiant heater. The remainder of the vacuum system consists of stainless steel tubing and 316 stainless steel fitings and valves manufactured by Swagelok. A vacuum pump manufactured by Sargent Welch is used to provide the necessary vacuum. A diffusion vacuum pump in the vacuum line directly prior to the mechanical vacuum pump provides additional vacuum. Samples are suspended from loop B of the electrobalance. Nichrome extension wire of 0.1 mm diameter is used to allow the sample to hang in the proper orientation to the radiant heater. A hook placed inside ice samples during formation or a suspension spring (see Figure 8) for carbon dioxide and hydrate samples is employed to attach the sample to the extension wire.

Hydrate Formation

The hydrate formation equipment is presented in Figure 9. A 303 stainless steel cell is used to form the methane hydrates (see Figure 10). O-rings are used at each end of the cell to insure sealing during formation. The accompanying threaded ram is used to compress the hydrates after formation and to extrude the hydrates from the formation cell. Hydrates are formed in the smooth portion of the cell. This section is 5 inches in length and 0.412 inches in diameter. After packing the hydrate sample has the proper dimensions necessary to be used in the dissociation experiments.

Constant temperature is maintained during the formation process by submerging the formation cell in a constant temperature bath filled with a fifty-fifty mixture of ethylene glycol and water. Maintenance of temperature in the bath is achieved with a combination of a Lauda IC-6 refrigeration unit and an adjustable model 1120 bath heater manufactured by VWR. A layer of insulation surrounds the bath to minimize heat input to the bath.

Pressure is monitored using a Heise pressure gauge with a range of 0.0-2000 PSI. A calibration curve for the gauge has been determined at the National Bureau of

Figure 9

Listing of Equipment

1. Thermocouple and indicator
2. VWR heater
3. Lauda refrigeration unit
4. Temperature bath and hydrate cell
5. Pressure gauge
6. Methane cylinder
7. Vacuum pump
8. Vent

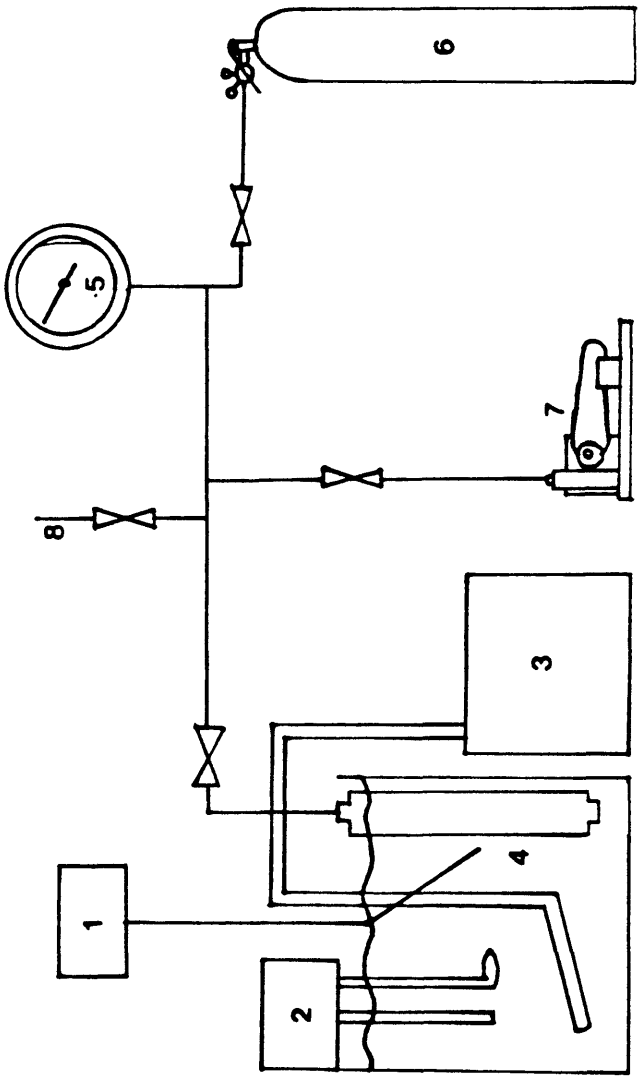

Figure 9
Hydrate Formation Apparatus

Figure 10

Hydrate Formation Cell

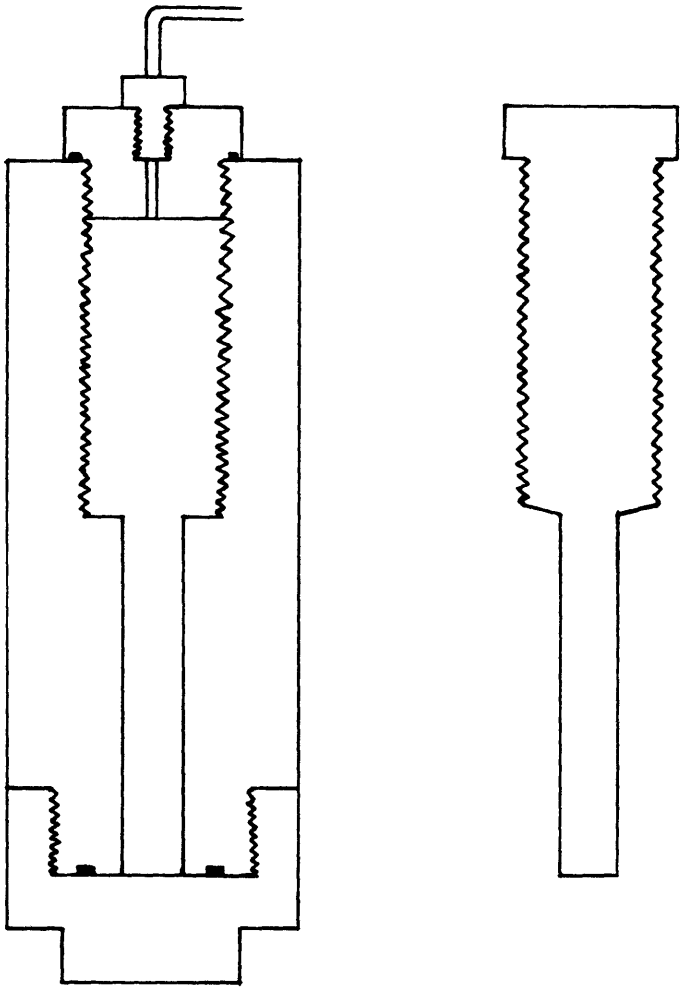

Standards in Boulder, Colorado (31). This curve was determined using a dead weight tester. The following empirical equation is used to correct pressure readings.

$$P_{actual} = 2.260835 + 0.9965814(P_{gauge}) + 0.000007(P^2_{gauge})$$

A mechanical vacuum pump is used to evacuate the associated stainless steel tubing and Swagelok 316 stainless steel fittings prior to hydrate formation.

The methane hydrates are formed using 99.97 per cent pure research grade methane and crystalline Colorado powder snow.

Experimental Procedure

Each of the three phases of the experimental work was completed using a separate procedure. Each of these procedures is briefly outlined below.

Bomb Calorimetry

In order to use the bomb calorimeter to make a determination on the insitu samples, first the equivalent heat of the calorimeter needs to be determined. This determination is made using benzoic acid. Secondly, the measured value of the equivalent heat was checked by testing two confirming unknowns. In the first calorimetry work the unknowns were camphor ($C_{10}H_{16}O$) and phenol (C_6H_5OH). The unknowns used in the later calorimetry work were napthalene ($C_{10}H_{22}$) and benzoic acid (C_6H_5COOH). After these two steps the hydrate samples were tested.

The following procedure was used to calibrate the bomb calorimeter and to test the confirming unknowns. The hydrate samples were tested following the same basic procedure except for a few changes.

1) Disassemble the calorimeter.
2) Weigh 2000 ± 0.5 grams of distilled water and place in the stainless steel bucket.
3) Measure approximately 10 centimeters of fuse wire. Connect the anodes together with the fuse wire using forceps to handle the wire.
4) Weigh to 0.1 milligrams, a sample of benzoic acid or confirming unknown and press into a pellet.
5) Place the pellet in the stainless steel cup and set in the calorimeter. Make sure the fuse wire is in contact with the sample.
6) Place 1.0 milliliter of deionized water in the bomb and seal.
7) Slowly charge the bomb with excess oxygen of between 25.0 and 28.0 atmospheres.
8) Place the bomb in the distilled water, connect the terminals of the ignition system, and allow the mechanical stirrer to operate for ten minutes to reach thermal equilibrium.
9) Take temperature measurements for a five minute preperiod. Take measurements every minute.
10) At the end of the fifth minute ignite the sample. Take temperature measurements at 45, 60, 75, 90, and 120 seconds after ignition. Thereafter, take

temperature measurements every minute until the rate of change of temperature with time is constant for five minutes. The temperature during the rise is read to +0.02 ^{0}C and to +0.005^{0}C during the preperiod and the postperiod.

11) Disconnect the bomb, vent the gases, and measure the length of unburned fuse wire.

The procedure is modified as follows for the hydrate samples. Steps 1-3 and 8-11 of the above procedure are followed, but steps 4-7 are replaced with these steps.

4) Place 1.0 milliliter of deionized water in the bomb
5) Weigh the bomb.
6) Place a sample of hydrate in a chilled stainless steel cup and set into the bomb, sealing quickly.
7) After allowing the hydrate sample to decompose, charge the bomb with enough excess oxygen to combust the methane, keeping in mind the combustion limits of methane (5.3 - 14.0 by volume).

Weighing Test

A procedure to determine the percentage of water converted to hydrate is outlined below. This method was tested in conjunction with bomb calorimetry to determine its usefulness. Only after confirming tests on portions of the same hydrate sample was the test independently used.

1) Form a hydrate sample.
2) Remove the hydrate sample from the formation cell after chilling on dry ice.
3) Place the sample in a chilled cup.
4) After zeroing the balance set the sample and cup on the balance pan.
5) Monitor the change in mass as the methane evolves leaving the water behind.
6) Determine the mass of the water in the hydrate sample.

Sample Preparation

The samples are formed in a cylindrical geometry. However, the mass of the sample to be used in the dissociation experiments is limited by the capabilities of the Cahn 2000 electrobalance. Keeping in mind the mass

constraint, solutions for an infinite cylinder and a finite cylinder (33) were used to determine the sample dimensions. The solutions used assume a zero initial temperature and conduction at the surface. A computer program was written for each solution and the results compared. A cylinder with a length to diameter ratio of five was found to very closely approximate an infinite cylinder. Based on this finding samples are formed in dimensions of 0.4 inches in diameter and 2.0 inches in length.

The ice samples were formed inside a length of capillary and removed for chilling. Cylinders of carbon dioxide were readily obtainable from a carbon dioxide supplier. These cylinders were not uniform, therefore a cork boring tool was used to shave the cylinders to the desired dimensions. Hydrate samples were formed in the previously described formation cylinder.

Hydrate Dissociation

The following procedure was used to collect the data on hydrate dissociation. The same procedure was used on the ice, carbon dioxide, and hydrate samples. However ice was mainly used to determine the radiant heat flux from the heater, and carbon dioxide was used to comfirm the flux.

1) Form a sample and chill on dry ice.
2) Allow the surface temperature of the heater to come to 200^{0}_{F}.
3) Calibrate the electrobalance.
4) Suspend the sample using the proper amount of tare weights.
5) Turn on the vacuum pump and put the hangdown tube and heater in place.
6) Take mass loss with time measurements using the strip chart recorder.

Hydrate Sample Formation

The Procedure to form hydrates is that developed by Holder (32). Slight modifications have been made to better meet the present experimental situation. The most significant change deals with the crystalline water used in the process. Holders' method employs the use of a heater in a beaker of water placed in a freezer. The water vapor condenses in fine crystals on the freezer walls and is then collected. This aspect of the procedure was not used but rather dry powder crystaline snow was collected following a Colorado spring storm. The snow was stored in a freezer maintained at -40^{0}F. The procedure is as follows:

1) Cool the formation cell on dry ice.
2) Cool the temperature bath to $-7^{o}C$.
3) Pack the formation cell with snow kept in the $-40^{o}F$ freezer.
4) Place the formation cell in the bath and evacuate the piping.
5) Slowly pressurize the system to 600 PSI with methane. Pressurize at a rate of 5 PSI per minute.
6) Raise the temperature of the bath to $1^{o}C$.
7) Allow forty-eight hours for the hydrates to form.
8) Remove the hydrate sample from the formation cell after chilling on dry ice.

Forty-eight hours was found to be sufficient for methane hydrate formation. This determination was made by observing when the rate of change of the pressure drop approached zero.

Results and Discussion

In Situ Hydrate Sample Testing

When the testing work was conducted, three of the four stainless steel cylinders contained gas hydrates. Samples were tested from all three of the cylinders. Table 4 shows the sample mass, sediment mass, and container source for all calorimetry experiments. The percent sediment and percent hydrate, or indication of apparent ignition, are presented in Table 5. Hydrate composition results of experiments conducted on shipboard and in other laboratories are included for completeness (see Table 6). It is interesting to note in Table 6 that the original test of the samples on shipboard indicated 13 mass percent hydrates and that 37 percent is the highest amount determined from these samples.

The first five samples tested were removed from stainless steel cylinder number one. The first three of these samples were taken from the section of the cylinder nearest the flange. The other two runs made on gas hydrates from this cylinder were done using samples from the cylinder bottom. The sample in this first cylinder was mostly white and slightly marbled with a light green color. No sediment particles were present in the sample color.

Table 4

Hydrate Sample Characteristics

Run Number	Source Cylinder	Sample Mass (gm)	Sediment Mass (gm)
1	1	8.729	0.092
2	1	2.960	0.027
3	1	3.802	0.100
4	1	4.784	0.211
5	1	1.588	0.105
6	2	2.940	0.060
7	2	2.135	0.078
8	2	1.814	0.102
9	3	4.619	2.590
10	3	9.274	5.696

Table 5

Calculated Hydrate Sample Characteristics

Run Number	Percent Sediment	Percent Hydrate
1	1.05	No ignition
2	0.91	No ignition
3	2.63	19.8
4	4.41	No ignition
5	6.61	16.7
6	2.04	No ignition
7	3.65	2.63
8	5.62	No ignition
9	56.07	No ignition
10	61.42	No ignition

Table 6

History of Sample Tests

Date	Percent	Location
2/18/82	13.1	Shipboard (13)
5/05/82	29.0	USGS Menlo Park (13)
10/12/82	37.2	USGS Menlo Park (13)
11/30/82	30.4	USGS Menlo Park (13)
8/30/84	19.8	CSM
9/03/84	16.7	CSM
9/07/84	2.6	CSM

The second cylinder was less than one third full. No attempt was made to obtain samples from different locations in this cylinder. The hydrate sample present in this cylinder was also white, but with no discoloration, giving the impression of a much smaller sediment content and much larger hydrate content than in the first cylinder. Runs labeled six through eight were conducted using sample from cylinder number two.

Two tests were done using hydrate from the third sample cylinder. The material in this cylinder contained a high sediment content which required larger sample masses. A very dark green appearance was associated with this sample of gas hydrate. This sediment formed chunks while drying as if a cementing process was occurring. However, the chunks could easily be crushed. In contrast, the sediment from the other two cylinders was a fine unconsolidated material after it was dried. Scanning electron microscopy was performed on the sediments from the samples after combustion. Micro-photograph 1 at a magnification of 1000X illustrates some of the residual matter present in the sediments, thereby giving credibility to the theory of anaerobic digestion as the source of the hydrated gases.

The results indicate that the first sample cylinder

Illustration 1

Marine Sediment

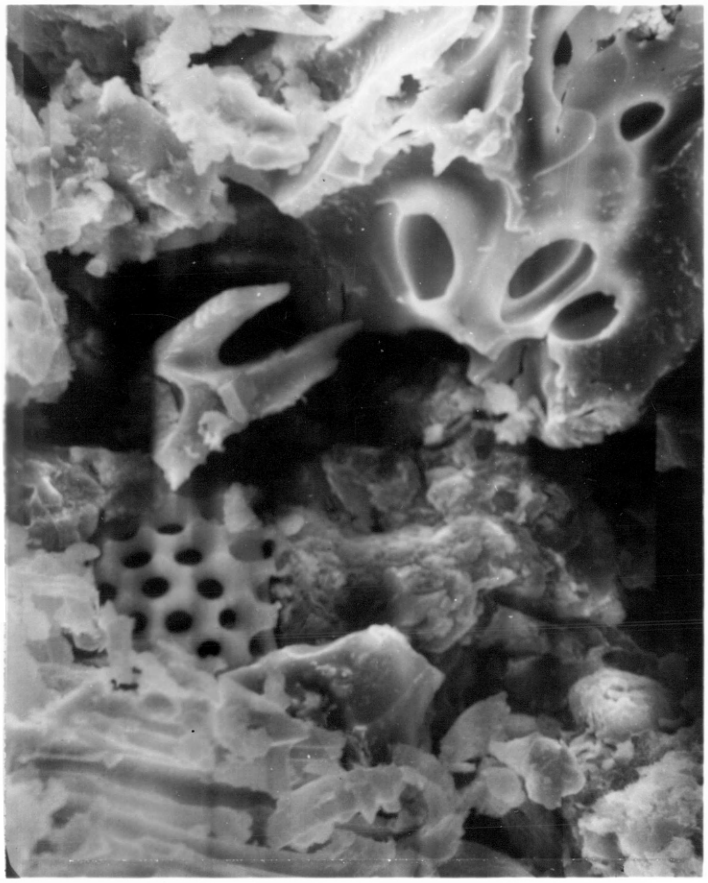

contained the highest percentage of gas hydrates. The calculated percentages were 19.8 and 16.7. Only one apparent ignition took place for the samples from cylinder number two. The calculated gas hydrate percentage was 2.63. No significant ignition took place for the samples from the third container.

These results indicate a much lower ratio of gas molecules to water molecules than the stoichiometric ratio of 1:5.75. Based on this fact it is concluded that the in situ hydrate samples have aged and decomposed since recovery from site 570 of the Deep Sea Drilling Project.

Gas analysis showed that the hydrate typically contained carbon dioxide and methane. These results are summarized in Table 7. Other hydrocarbon gases were present in some samples. These gases included ethane, propane, n-butane, and isobutane. It is interesting to note that several gases were detected in the second gas chromatographic run but not in the first. Since the system is purged prior to each test, these gases are definitely present. Possibly the gases are condensed liquids at the initial pressure for run one and then partially vaporized for run two. These gases were typically present in percentages less than one percent. By examining the gas analysis data carefully, evidence of partial combustion may

Table 7

Gas Analysis

Run Number	Test Number 1		Test Number 2	
1	n-butane	0.07	n-butane	0.71
	CO_2	3.85	CO_2	3.98
	CH_4	96.08	CH_4	94.55
			i-butane	0.48
			ethane	0.28
2	CO_2	1.98	CO_2	2.19
	CH_4	98.02	CH_4	97.81
3	CO_2	99.02	CO_2	99.01
	CH_4	0.98	CH_4	0.99
4	CO_2	7.33	CO_2	7.43
	CH_4	92.67	CH_4	92.57
5	CO_2	100.00	CO_2	100.00

Table 7 Continued

Run Number	Test Number 1		Test Number 2	
6	n-butane	0.39	n-butane	0.52
	i-butane	0.31	i-butane	0.37
	propane	0.75	propane	3.00
	CO_2	8.28	CO_2	7.71
	CH_4	90.27	CH_4	86.07
			ethane	2.33
7	CO_2	90.97	CO_2	91.21
	CH_4	9.03	CH_4	8.79
8	n-butane	0.43	n-butane	0.46
	i-butane	0.31	i-butane	1.13
	propane	0.75	propane	0.75
	CO_2	4.79	CO_2	4.87
	CH_4	92.55	CH_4	91.32
	ethane	1.16	ethane	1.45
9	CO_2	55.39	CO_2	55.17
	CH_4	44.61	CH_4	44.83
10	CO_2	76.24	CO_2	76.23
	CH_4	23.76	CH_4	23.77

be discerned. Runs nine and ten are good examples of this phenomenon. For these runs combustable gas must have been present in such low concentrations that total combustion was not possible. Total combustion took place on runs three and five, while nearly total combustion occurred on run seven. For the other runs a definite statement as to extent of combustion cannot be made.

The results of the calibration runs to determine the energy equivalent of the oxygen bomb are presented in Table 8. Two test runs were made on samples for which the heat of combustion is known. Phenol and camphor were the compounds used for these tests and are also included in Table 8. The results of these calibration checks were tested against reported literature values for the heat of combustion. Based on these comparisons the results of the calorimetry work are accurate to within 2%.

Table 8

Calibration and Testing

Benzoic Acid

Run Number	Energy (cal/^{o}C) Equivalent
1	2594.9
2	2536.0
3	2479.0
4	2503.3
5	2462.1

Check Runs

Compound	Calculated Value (kcal/gmol)	Reported Value (kcal/gmol)	Percent Error
Phenol	-279.6	-729.8	0.027
Camphor	-1428.1	-1410.96	1.200

Dissociation Experiments

The incident radiant energy produced by the heater was determined using ice. Cylinders of ice were prepared from deionized water in the geometry approximating an infinite cylinder. The geometry was determined from infinite and finite cylinder solutions taken from Conduction Of Heat In Solids by Carslaw and Jaeger (33). Each cylinder was chilled after formation and its dimensions measured prior to the dissociation experiment. The change in mass of the sample with time was monitored using a strip chart recorder. This data was used to calculate the position of the moving front with time. By assuming the applicability of the long time ablation model, the data was used to determine the energy flux from the heater which was incident on the sample. The results of these experiments (see Table 9) indicated that the incident energy flux is 1.0242 KW/M^2 with a standard deviation of 0.0430 KW/M^2. This value was arrived at by averaging the flux value calculated from mass loss data at one minute intervals for each run, and then averaging the results of the experiments.

The assumption of the applicability of the ablation solution is a good one. The shape of the mass loss with time curve is a straight line. Therefore, the position of

Table 9

Radiant Heater

Calibration Results Using Ice

Run	Calculated Flux (KW/M^2)
1	1.0386
2	0.9585
3	1.0527
4	1.0055
5	1.0657

the moving front with time calculated from this data is also a straight line. A straight line for the position of the moving front with time is predicted by the ablation model. The lines predicted by the ablation model for various values of incident energy flux and the calibration data are parallel (see Figure 11). The fact that the data is parallel to the model predictions further indicates the applicability of the ablation model.

Carbon dioxide was used to check the value for the energy flux determined from the ice experiments. Carbon dioxide cylinders were prepared in the same geometry as the ice cylinders. Carbon dioxide has a much smaller heat of sublimation, therefore the slope of the mass loss with time curve was much greater than that for ice. The slope of this curve was constant with time.

Since this curve was much steeper, the slope of the curve was used to determine the incident energy flux. To use the slope value, the change in mass with time, the Selim-Sloan long time ablation model was differentiated. The differentiation of the long time solution is presented below. For full details of the development of the long time ablation model see Appendix A.

$$X = (\nu/1+\nu) * (Ft/\rho\lambda)$$

$$dX/dt = (\nu/1+\nu) * (F/\rho\lambda)$$

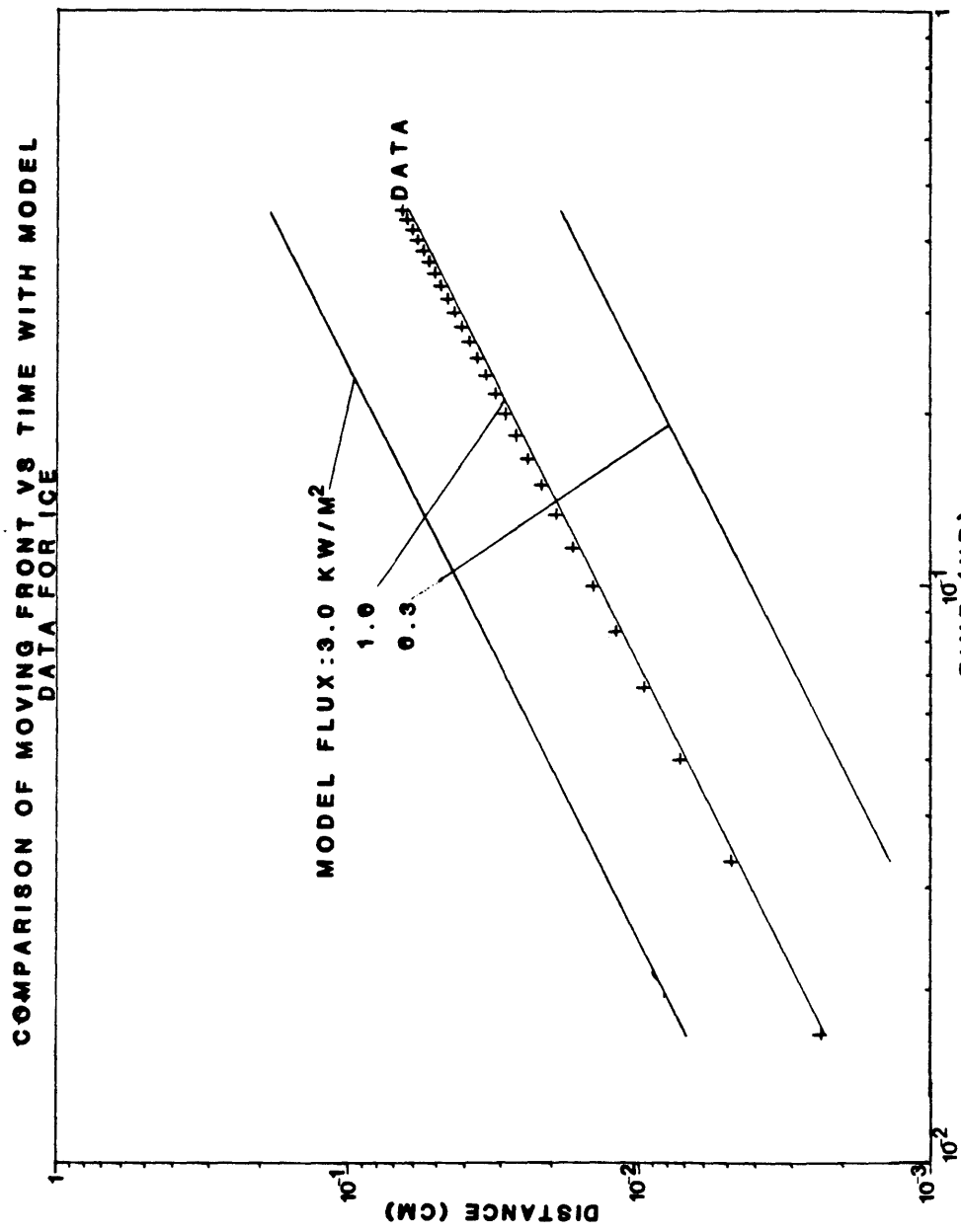
COMPARISON OF MOVING FRONT VS TIME WITH MODEL DATA FOR ICE
MODEL FLUX:3.0 KW/M2
1.0
0.3
DATA
DISTANCE (CM)
TIME (HR)
1
10-1
10-2
10-3
10-1
10-2
1

Figure 11

The mass of a planar object at any time is:

$$M = AX\rho$$

The change in mass with time of this object is:

$$dM = A\rho\, dX$$

The derivative of the long time ablation model upon substitution becomes:

$$dM/dt = (\nu/1+\nu) * (AF/\lambda)$$

A cylindrical geometry was used, therefore, the area is the surface area of the side of a cylinder. Thus, the appropriate equation is:

$$dM/dt = (\nu/1+\nu) * (2\pi RLF/\lambda)$$

To apply this equation the length and radius of the sample need to be known. Prior to beginning the dissociation experiment the length and diameter of the carbon dioxide cylinder was measured. The length does not change during the course of an experiment, however the radius decreases. Based upon the mass loss up to the time of the slope measurement and using the initial radius, the radius at the time of the slope measurement was calculated. Several experiments were conducted with carbon dioxide and the calculated value of the incident energy flux on the sample was 1.0168 KW/M^2 with a standard deviation of 0.0314 KW/M^2. The results of these experiments are presented in Table 10.

Table 10

Heater Calibration

Check With Carbon Dioxide

Run	dM/dt (gm/min)	Mass Loss (gm)	Calculated Flux (KW/M^2)
1	0.180	1.000	1.0467
2	0.174	0.750	1.0025
3	0.136	0.350	1.0303
4	0.154	0.600	1.0473
5	0.165	1.000	1.0082
6	0.171	1.000	1.0483
7	0.139	0.600	0.9650
8	0.174	1.000	0.9864

The hypothesis that the difference between these two mean flux determinations was equal to zero was checked using statistical methods. This hypothesis was checked assuming that the standard deviations of the true means were unknown and not equal. The hypothesis was also checked assuming that the standard deviations of the true means were equal but unknown. In each case the hypothesis was confirmed. Therefore, the energy flux incident on the sample from the heater was known. The flux value from the ice experiments was used in all calculations involving the hydrate dissociation calculations. This value was used since the physical properties of ice more closely approximate those of hydrate than do those of carbon dioxide.

Since the hydrates recovered from the ocean floor at site 570 of the Deep Sea Drilling Project were deemed insufficient for experimental testing of the ablation model, hydrates were produced in the laboratory. Tests were conducted on these laboratory hydrates to determine the percentage of snow converted to hydrate and that which remained as water in the form of ice. Bomb calorimetry was again used as a method of testing.

The bomb calorimeter was again calibrated with benzoic acid and the equivalent energy value was found to be 2497.7

cal/^{0}C with a standard deviation of 10.51 cal/^{0}C. Two unknown samples were used to check the calibration. Napthalene was one of the unknowns and its experimentally determined heat of combustion was 2.24 percent in error compared to the reported literature value. The other unknown was benzoic acid and its experimentally determined heat of combustion was 2.97 percent in error compared to the reported literature value. The results of this calibration are presented in Table 11.

A new method of testing was also used. This method involved placing a sample of hydrate on a balance and measuring the mass of methane evolved during dissociation. The mass of the water which remained could then also be measured. With these two values the percentage of hydrate is easily calculated. The two tests were used in conjunction with one another, and both tests were conducted on portions of the same hydrate sample. Thus, each test confirmed the other. The results of these comparative tests are presented in Table 12. A gas chromatographic test was conducted on the combustion gases of bomb calorimeter run 1, and the results indicated complete combustion as had been the case with runs 3, 5 and 7 of the previous calorimetry work.

Laboratory hydrates were now formed with the

Table 11

Calibration and Testing

Benzoic Acid

Run Number	Energy (cal/^{o}C) Equivalent
1	2515.9
2	2493.5
3	2488.8
4	2493.9
5	2497.7

Check Runs

Compound	Calculated Value (Kcal/gmol)	Reported Value (kcal/gmol)	Percent Error
Naphthalene	-1259.43	-1231.8	2.24
Benzoic acid	-794.14	-771.24	2.97

Comparative Tests

On Laboratory Hydrates

Run	Percent Hydrate Bomb Calorimetry	Percent Hydrate Mass Loss Test	Percent Difference
1	32.0	31.8	0.63
2	63.9	61.0	4.57
3	31.1	28.8	5.67

anticipation of making mass loss measurements using the electrobalance apparatus. Several samples were obtained using the formation procedure, however all samples did not maintain the desired shape upon removal from the formation cell. Measurements on the samples which fractured into several pieces were made. The measurements involved determing the mass of methane and water in each sample. In this way a judgment on the percentage of hydrate in each sample used on the electrobalance could be made. The results of these tests are tabulated in Table 13. During the formation of all laboratory hydrate samples, the drop in methane pressure in the system tubing was monitored. In all cases the pressure drop associated with hydrate formation was in the range of 275 to 412 Kilopascals. Therefore, the samples which were tested using the mass loss procedure were deemed to be representative of those used in the electrobalance experiments and are 70.0 to 90.0 percent hydrate by mass. The mass loss method of determining the percentage of hydrate was used for two reasons. First, its reliability had been confirmed by comparison with the bomb calorimetry method and secondly, this method was more easily and quickly accomplished.

Three successful dissociation experiments yielded data which could be compared to the long time ablation model. A

Table 13

Mass Loss Tests

On Laboratory Hydrates

Sample Number	Percentage Hydrate Mass Loss Test
1	89.38
4	85.06
5	70.21
7	83.11

graphical comparison between the model prediction and the data is made in Figures 12, 13 and 14. The data and the long time ablation model predictions of the moving front are both linear functions of time. The data and the model prediction are also parallel. The constant factor $(\nu/1+\nu)$ in the model, with ν being the Stefan number, is assumed to be equal to one. This assumption is based on calculations of the Stefan number and is also confirmed by the parallelism of the data and the model prediction. The long time ablation model underpredicts the data by an average 6.042 percent for data set one, 8.503 percent for data set two, and 9.89 percent for data set three.

The model prediction was calculated using a value for the heat of dissociation of 2618.8 W.s/gm as calculated in Appendix B. This value was calculated for hydrates in equilibrium at the formation conditions. These hydrates have a ratio of 1 methane molecule to 6.15 water molecules or 93.5% hydrate by mass. The heat of dissociation changes very little with change in the mass fraction of hydrate. For samples of 80% hydrate by mass the heat of dissociation would be 2652.7 W.s/gm. This small 1.3% change in heat of dissociation has negligible effect on the model prediction.

If the uncertainties in the value of the radiant energy flux and the value of the heat of sublimation are

propogated (34) through the Selim-Sloan model the error resulting in the predicted values would be plus or minus five percent. Based on calculations using the propogation of errors method, the expected experimental error is less than fifteen percent with the expected error decreasing as time increases. Differences between the Selim-Sloan prediction and the data are in the range expected with a model of this sort.

Samples which approximate an infinite cylinder were used in the dissociation experiments, end effects however may contribute to the difference between the data and the model prediction. End effects would contribute to a larger mass loss with time thereby indicating a greater movement in the dissociation front with time.

The time for dissociation to begin, t_{sd}, (see Appendix A) was calculated using representative hydrate properties and was found to be approximately 30 seconds. This time was easily consumed during sample suspension, therfore it is assumed that the surface temperature of the hydrate is at the dissociation temperature as the experiment begins.

The absorptivity properties of the three substances experimented on were investigated. Data was found on the refractive index and the extinction coefficient as a function of the wavelength of infrared radiation (35,36).

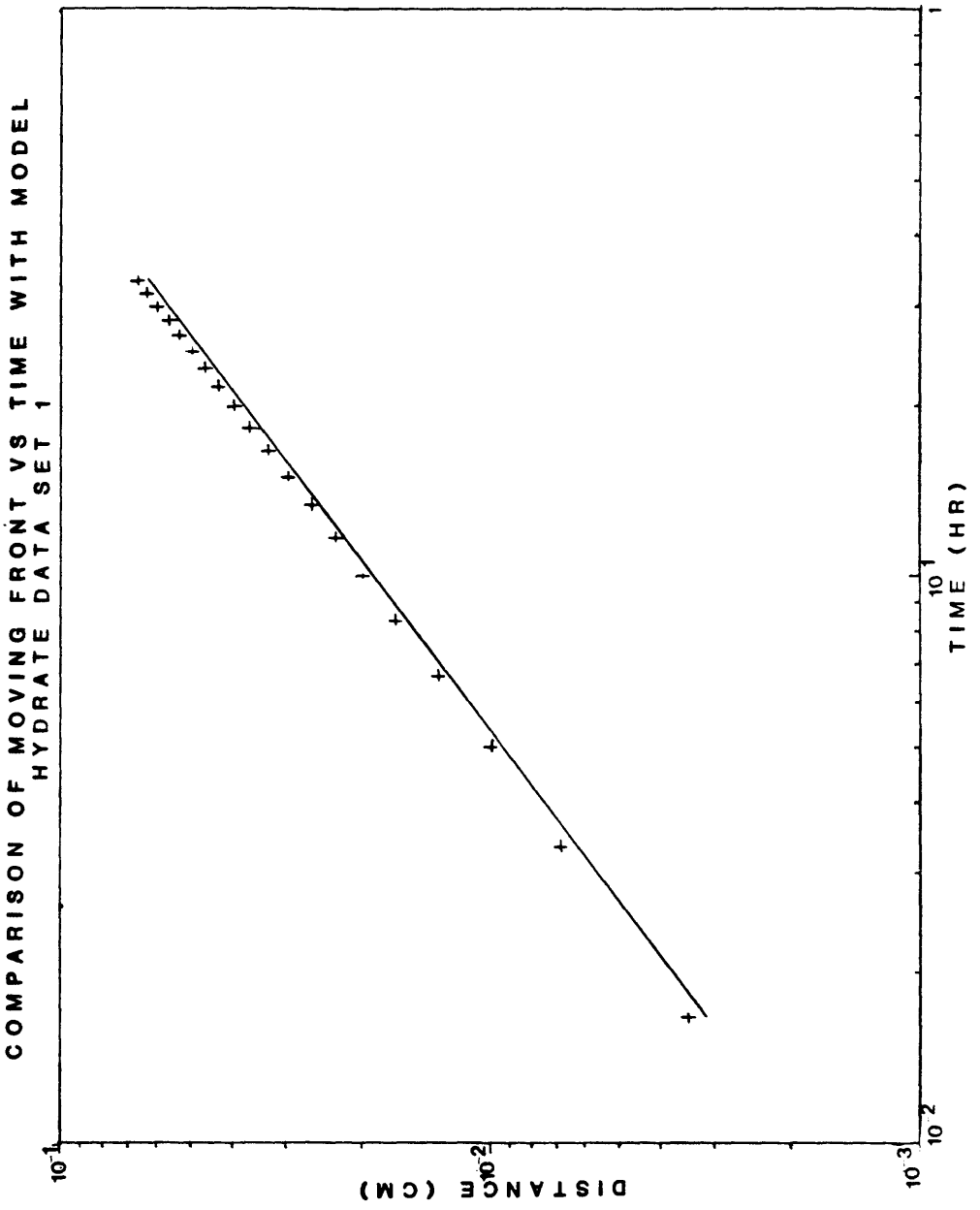
COMPARISON OF MOVING FRONT VS TIME WITH MODEL
HYDRATE DATA SET 1
DISTANCE (CM)
TIME (HR)
10^-1
10^-2
10^-3
10^1

Figure 12

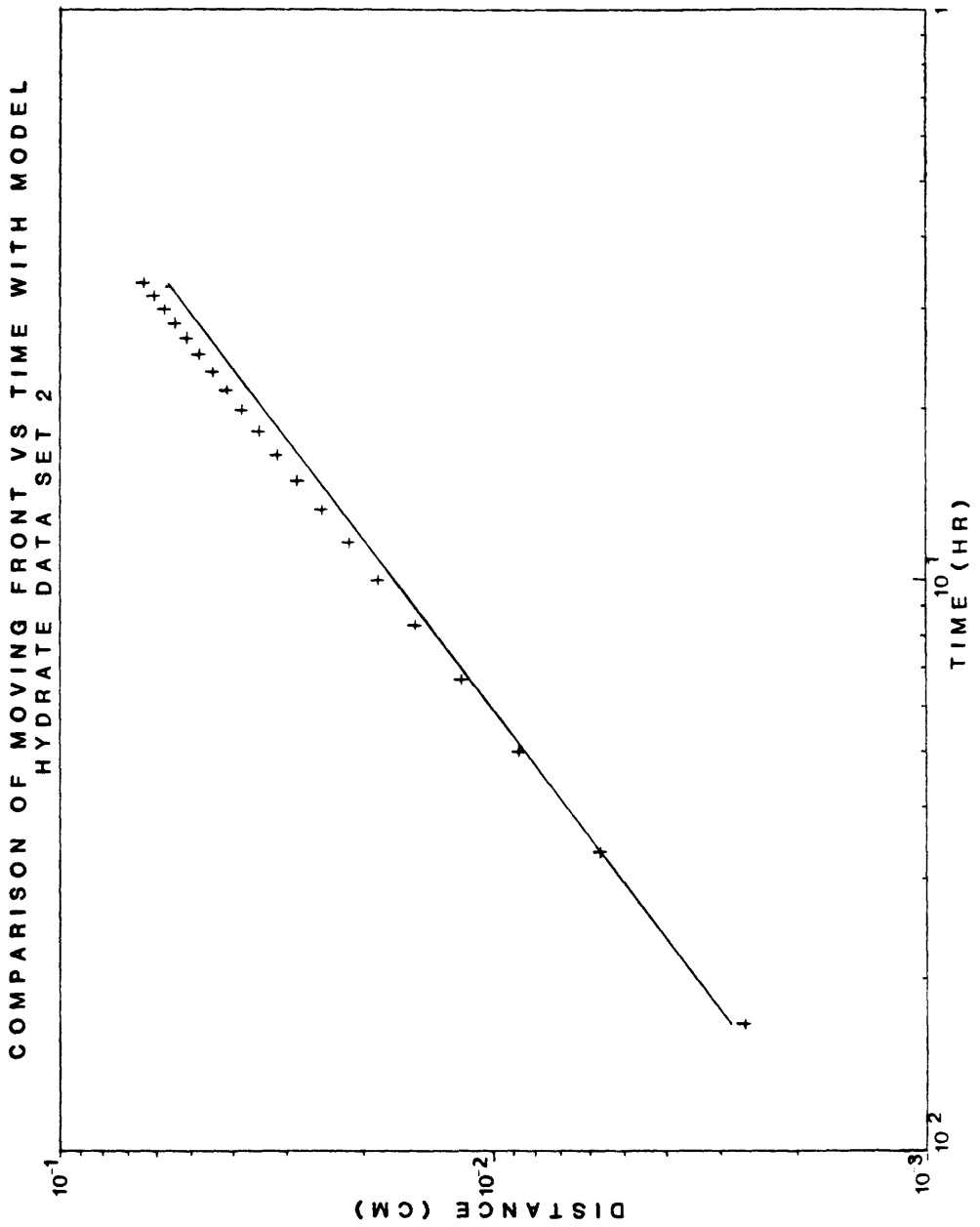
COMPARISON OF MOVING FRONT VS TIME WITH MODEL
HYDRATE DATA SET 2
DISTANCE (CM)
TIME (HR)
10^{-1}
10^{-2}
10^{-3}
10^{-2}
10^{-1}
1

Figure 13

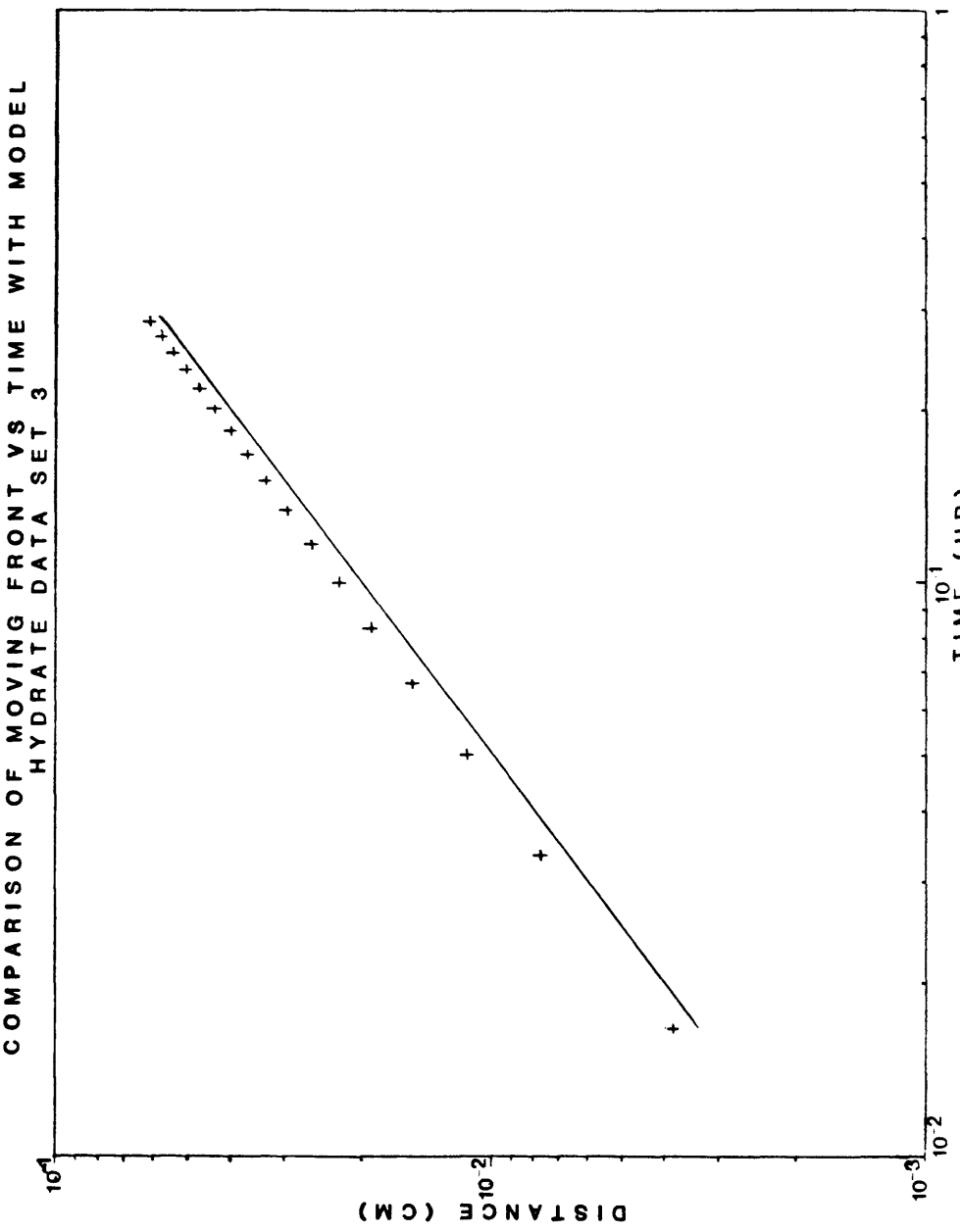
COMPARISON OF MOVING FRONT VS TIME WITH MODEL
HYDRATE DATA SET 3
DISTANCE (CM)
TIME (HR)
10^-1
10^-2
10^-3
10^-2
10^-1
1

Figure 14

This data could only be uncovered for ice and solid carbon dioxide. The wavelength of greatest intensity was determined using Wiens' law. Data for this wavelength was then used in the Fresnel equation for incident radiation on a body. In this way a value for the reflectivity of ice and solid carbon dioxide was determined. The transmissivity of ice was approximated as zero and that of solid carbon dioxide was assumed to also be zero.

Since the sum of the transmissivity, the reflectivity, and the absorptivity is defined to be equal to one, a value for the absorptivity was now determined. Based on these calculations the absorptivities for ice and solid carbon dioxide were found to be 0.97 and 0.98 respectively. Considering these values it would be anticipated that the experimentally determined energy flux values using ice and solid carbon dioxide would be close to the same value. As has already been pointed out, this was the case.

Data to make these calculations for methane hydrate was not available. Therefore, the value calculated for ice was assumed to be representative of the value for methane hydrate. Based on this assumption the flux calculated from the ice experiments was assumed to be that incident on the methane hydrate samples. If the absorptivity of the hydrate samples were greater, a larger movement in the

front with time would be observerd.

A constant pressure of 1.5 torr was maintained by the vacuum pump during all dissociation experiments. A pressure drop calculation was made using appropriate formulas from Crane (37). This pressure drop calculation confirmed that only thermal radiation stimulation was causing dissociation. If a good vacuum had not been maintained around the sample, convection heat transfer would have been important.

A dry silicone lubricant with Teflon was used to facilitate the removal of the hydrate samples from the formation cell. The amount of lubricant used was kept to a minimum and did not seem to effect the gathering of the dissociation data. The Teflon was white and blended with the hydrate sample. It was therefore, difficult to judge the amount of Teflon on the sample through visual inspection. When weighing tests were made very small amounts of Teflon could be seen floating on the water left after dissociation.

During two of the dissociation experiments with methane hydrate for which data was not reported, an insufficient vacuum was maintained. This problem resulted from a lack of vacuum grease sealing a ground glass joint in the diffusion pump. It was noticed during these runs,

after the heater was quickly removed, that the surface of the sample seemed to be boiling. What was taking place was rapid ablation. Since the vacuum was not sufficient, a greater energy transfer to the hydrate sample was taking place due to conduction and convection. Upon close examination the water could be seen to blow from the hydrate surface as the methane gas was liberated. This phenomena further confirms the theory of ablation.

Another interesting phenomena was also observed while conducting this work. During the development stage of the experiment, methane hydrate samples were allowed to drop directly from the formation cell into liquid nitrogen but this procedure was later discontinued. After chilling, the sample was dissociated. Upon dissociation an S shaped curve was drawn upon the strip chart recorder paper, before the afore mentioned dissociation represented by a staight line began. The liquid nitrogen was obviously the cause. It is believed that the nitrogen molecules were somehow diffusing into the methane hydrate sample or into fissures in the hydrate sample. Nitrogen is a hydrate former, however, it does not seem likely that the nitrogen molecules could diffuse into empty cavities which had already formed. The samples of methane hydrate on which this phenomena was observed where not of the quality used

in later experiments, since a much shorter formation period was allowed.

Conclusions

1. Tests on the site 570 hydrates have been made using bomb calorimetry. The results indicate that these samples were 2-20 percent hydrate by mass. These results indicate a much lower ratio of gas molecules to water molecules than the stoichiometric ratio of 1:5.75, indicating that the samples have aged and decomposed since recovery.
2. An apparatus has been constructed to take dissociation data. This experimental apparatus has been shown to take acceptable data by running experiments with ice and solid carbon dioxide.
3. Satisfactory methane hydrates were produced in the laboratory for dissociation experimental work. These hydrates were tested using bomb calorimetry and a mass loss procedure to determine their usefulness.
4. Experimental data was taken on methane hydrate dissociation. This data was compared with the Selim-Sloan ablation model. This model was seen to under-predict the data by 8-10 percent, but the general trend of the dissociation data was predicted by the model.
5. The model acceptably determines the dissociation of the methane hydrates and would be a satisfactory model to incorporate into a production scheme.

Recommendations

1. Hydrates should be made in consolidated sediment and experiments run with the electrobalance apparatus. In this way the Selim-Sloan model may be extended to model hydrate dissociation for the conditions of insitu hydrates.
2. A personal computer should be interfaced with the electrobalance and the electronic manometer to better facilitate the collection of data.
3. A better formation cell should be constructed so that the removal of the hydrates is an easier process and so that the samples remain in a usable piece. A two piece mold may be a possible alternative.

References Cited

1. Lewin and Associates, Inc., Handbook of Gas Hydrate Properties and Occurrence, Washington D.C., U. S. Printing office, (1983). (DOE/MC/19239-1546)
2. Sloan, E.D., "Shore Based Laboratory Experimental Measurements On A Gas Hydrate Sample Recovered At Site 570", Initial Reports of the Deep Sea Drilling Project, v. LXXXIV, p695-698, (1985)
3. Brown, J.F., Scientific American, v207(1), p82-92, (1962)
4. Stackelberg Von, M. and Muller, H.G., J. Chem. Phys., v19, p1319, (1951)
5. Claussen, W.F., J. Chem. Phys., v19, p259, (1951)
6. Pauling, L. and Marsh, K.E., Proc. Nat'l Acad. Sci. U.S., v38, p 112, (1952)
7. Davy, H., Phil. Trans. Roy. Soc., v101, p155, (1811)
8. Faraday, M.,Quart. J. Sci., v15, p71, (1823)
9. Claussen, W.F., J. Chem. Phys., v19, p1425, (1951)
10. Hammerschmidt, E.G., Ind. & Eng. Chem., v26, n8, p851, (1934)
11. Waals Van der, J.H. and Muller, H.G., Mol. Phys., v1, p91, (1958)

12. Makogen, Y., Hydrates of Natural Gas, Pennwell Publishing Co., Tulsa, Oklahoma, p7, (1981)

13. Kvenvolden, K.A., Claypool, G.E., Threlkeld, C.N., and Sloan, E.D., Geochemistry of a Naturally Occurring Massive Marine Gas Hydrate, Advances in Organic Geochemistry, Pergamon Press (in press), London, (1984)

14. Sunner, S. and Mansson, M., Combustion Calorimetry, Pergamon Press, Oxford, P400-403, p415-416, (1979)

15. Deaton, W.M. and Frost, E.M., U.S. Bureau of Mines Monograph, No. 8, 25-27, (1946)

16. Villard, P., Ann. Chem. et Phys., 11, 353-360, (1897)

17. Nagayev, V.B., Gritserko, A.I., and Murin, V.I., Eighth All-Union Conference on Calorimetry and Chemical Thermodynamics, Inonovo, Proceed. 1-NOR, 58, (1979)

18. Cherskii, N.V., Groysman, A.G., Nikitina, L.M., and Tserov, V.P., Doklady Akademee Nauk SSSR, 265(1), 185-189, (1982)

19. Sloan, E.D. and Callanan, J.E., GRI-81/0102, Final Report, "Heat Capacity Measurements on Structure I and Structure II Pure Hydrates at Low Pressures and Below Room Temperature", (1983)

20. Cherskii, N.V., Groysman, A.G., Tserov, V.P., and

Nikitina, L.M., Doklady Akademii Nauk SSSR (Geol), v270(4), p949-952, (1982)

21. Stoll, R.D. and Bryan, G.M., Journal of Geophysical Research, 84(No. B.4), 1629-1634, (1979)
22. Holder, G.D., Angert, P.F., John, V.T., and Yen, S.L., Journal of Petroleum Technology, v34, 1127-1132, (1982)
23. Rose, W. and Plannkuch, H.O., "Production Scheme For Deep Water Hydrate Deposits", SPE 11106, New Orleans, LA., (Sept 1982)
24. Kamath, V.A. and Godbole, S.P., "Evaluation of Hot Brine Stimulation Technique For Gas Production From Natural Gas Hydrates", SPE 13596, Bakersfield, CA., (March 1985)
25. McGuire, P.L.,"Methane Hydrate Gas Production BY Thermal Stimulation",Fourth Canadian Permafrost Conference, Calgary, Alberta, Canada, (March 1981)
26. Cherskii, N.V. and Bonarev, E.A., Doklady Akad. Nauk. SSSR, 203(3), p550-552, (1972)
27. Holder, G.D. and Angert, P.F., "Simulation of Gas Production From a Reservoir Containing Both Gas Hydrates and Free Natural Gas", SPE 11105, New Orleans, LA., (Sept 1982)
28. Verigin, N.N., Khabibullin, I.L., and Khalikov, G.A.,

Izvestiya Akademii Nauk SSSR, 1, p174-177, (1980)

29. Selim, M.S. and Sloan, E.D., "Modeling of the Dissociation of an In-Situ Hydrate", SPE 13597, Bakersfield, CA., (March 1985)

30. Parr Calorimeter Model 1341 Operation Manual, Parr Instrument Company

31. Guissani, A., Thesis #2461, Colorado School of Mines, p86, (1981)

32. Holder, G.D., Monthly Report Number 1, DOE Contract Number DE-AC21-83MC20013, "Laboratory Analysis of Gas Hydrate Cores for Evaluation of Reservoir Conditions", (August 1983)

33. Carslaw, H.S. and Jaeger, J.C., Conduction of Heat in Solids (2nd Edition), Oxford Press, London, p.203, (1959)

34. Taylor, J.R., An Introduction to Error Analysis, The Study of Uncertainties in Physical Measurements, University Science Books, Mill Valley, California, p 40, (1982)

35. Pepper, S.W., "Absorption of Infrared Radiation by Ice Cryodeposits", NASA Technical Note, NASA-TN-D-5181, p 17, (1969)

36. Egan, W.G. and Spagnola, F.A., "Complex Index of Refraction of Bulk Solid Carbon Dioxide", Applied

Optics, V 8(11), p 2359-60, (1969)

37. Flow of Fluids Through Valves, Fittings and Pipe, Crane Technical Paper No. 410, Crane Co., New York, p 46, (1980)

38. Goodman, T.R., "Application of Integral Methods to Transient Nonlinear Heat Transfer", Advances in Heat Transfer, vl, p 51-122, (1958)

39. Goodman, T.R., "The Heat Balance Integral and Its Application to Problems Involving a Change of Phase", ASME Trans., v80, p 335-342, (1958)

40. Schlichting, H., Boundary Layer Theory, McGraw-Hill, New York, (1968)

41. Schlichting, H. and Ulrich, A., "Zur Brechnung Umschlages Laminar-turbulent, Jahrbuch d. dt. Luftfahrtforschung", vl, p 8-35, (1942)

42. Pholhausen, K., "Zur naherungsweisen Integration der Differentialgleichung der laminaren Reibungschicht", ZAMM, vl, p252-268, (1921)

43. Chapman, A.J., Heat Transfer (third edition), MacMillan Publishing Co., New York, P 584, (1974)

44. Keenan, J.H. and Keyes, F.G., Thermodynamic Poperties of Water, John Wiley and Sons, New York, p 112, (1969)

45. Maass, O. and Barnes, W.H., "Some Thermal Constants of Solid and Liquid Carbon Dioxide", Proc. Roy. Soc.,

Alll, p 224-244, (1926)

46. Giauque, W.F. and Egan, C.J., "Carbon Dioxide. The Heat Capacity and Vapor Pressure of the Solid. The Heat of Sublimation. Thermodynamic and Spectroscopic Values of Entropy.", Journal Chemical Physics, V5., p 45-54, (1937)

47. Cook, T. and Davey, G., " The Density and Thermal Conductivity of Solid Nitrogen and Carbon Dioxide", Cryogenics, v16(6), p 363-369, (1976)

48. Falabella, B.J. and Vanpee, M, "Experimental Determination of Gas Hydrate Equilibrium Below the Ice Point", Industrial and Engineering Chemistry Fundamentals, v13, p 228-231, (1974)

49. Siegal, R. and Howell, J.R., Thermal Radiation Heat Transfer (2nd edition), McGraw-Hill, New York, p 91-100, 157, (1981)

Appendix A

Ablation Model

The mathematical formulation and solution of the Selim and Sloan (29) model of dissociation of an in-situ hydrate is presented in this appendix. This presentation is a portion of the paper presented by the authors at the Society of Petroleum Engineers 1985 California Regional Meeting held in Bakersfield, California, March 27-29,1985.

Mathematical Formulation

Consider a hydrate body initially at a uniform temperature T_i and occupying the semi-infinite region $0<x<\infty$ At time t=0 a constant heat flux F is applied to the boundary surface at x=0. Dissociation starts and as a result the boundary surface moves in the positive x-direction. Meanwhile, the temperature of the boundary rises from T_i to T_s which is the temperature in equilibrium with the prevailing pressure. Thereafter, the temperature of the moving boundary remains constant at T_s. To simplify the analysis, it is assumed that the water resulting from the dissociation process is completely removed from the surface immediately on formation. Effectively the gas blows the water away from the surface. Such an assumption

is usually encountered in ablation problems (38). There will therefore be no liquid phase over the dissociation surface and one need only consider the heat transfer problem in the undissociated solid phase.

Let t_{sd} be the time required for the boundary surface to reach the equilibrium temperature T_s. For moderately large values of heat input, F, t_{sd} will be fairly small so that the motion of the boundary surface may be ignored during the initial period. Thus for $t<t_{sd}$ the problem may be regarded as a fixed-boundary problem while for $t>t_{sd}$ the problem becomes a moving-boundary problem. The fixed-boundary problem may then be regarded as a heating problem preceding dissociation. The appropriate differential equations and associated boundary and initial conditions are given by:

for $t<t_{sd}$

$$\frac{\partial T}{\partial t} = \alpha \frac{\partial^2 T}{\partial x^2} \qquad 0<x<\infty \qquad ,t>0 \qquad (1)$$

$$-k \frac{\partial T}{\partial x} = F \qquad x=0 \qquad ,t>0 \qquad (2)$$

$$T = T_i \qquad x=\infty \qquad ,t>0 \qquad (3)$$

$$T = T_i \qquad 0<x<\infty \qquad ,t=0 \qquad (4)$$

for $t>t_{sd}$

$$\frac{\partial T}{\partial t} = \alpha \frac{\partial^2 T}{\partial x^2} \qquad X(t)<x<\infty \quad ,t>0 \qquad (5)$$

$$T = T_s \qquad x=X(t) \quad ,t>0 \qquad (6)$$

$$-k \frac{\partial T}{\partial x} + \rho\lambda \frac{dX}{dt} = F \qquad x=X(t) \quad ,t>0 \qquad (7)$$

$$T = T_i \qquad x=\infty \quad ,t>0 \qquad (8)$$

$$T = f(x) \qquad 0<x<\infty \quad ,t=t_{sd} \qquad (9)$$

where the function f(x) is obtained from the solution of the fixed-boundary problem.

Solution

Goodman (39) presented an approximate solution to an ablation problem similar to the problem encountered in the present study. This solution utilizes the heat-balance integral method together with a second-degree polynomial approximation for the temperature profile. The method is based on the von Karman-Pohlhausen momentum integral technique used in the analysis of boundary layers (40). As pointed out by Schlichting and Ulrich (41), the use of a higher degree polynomial results in better approximations to the exact solution. It seems natural, therefore, to improve Goodman's method which is based on a polynomial of the second degree (P 2-method) by selecting one of a higher

order. The additional coefficients can then be used to satisfy additional compatibility conditions at the boundary surface and at the edge of the thermal layer. Following Pohlhausen (42), a polynomial of the fourth degree will be used in the present solution (P 4-method). The main advantage of the P 4-method lies in the circumstance that the higher spatial derivatives of the temperature profile are obtained with an increased degree of precision, as compared with the P 2-method.

One first solves the fixed-boundary problem described by Eqs. (1) through (4). Thus, the heat-balance integral is obtained by integrating Eq. 1 over the thermal layer from x=0 to x=δ(t). This gives

$$\frac{d}{dt}(\theta - T_i\delta) = -\alpha \frac{\partial T(0,t)}{\partial x} \tag{10}$$

where

$$\theta = \int_0^\delta T \, dx \tag{11}$$

Now assume that T can be represented by a fourth-degree polynomial in x of the form

$$T = a_0 + a_1 x + a_2 x^2 + a_3 x^3 + a_4 x^4 \tag{12}$$

where the coefficients a_i may depend on t. These are determined from the following five conditions:

$$\frac{\partial T\ (0,t)}{\partial x} = -F/k \tag{13}$$

$$T\ (\delta,t) = T_i \tag{14}$$

$$\frac{\partial t\ (\delta,t)}{\partial x} = 0 \tag{15}$$

$$\frac{\partial^2 T\ (\delta,t)}{\partial x^2} = 0 \tag{16}$$

$$\frac{\partial^3 T\ (\delta,t)}{\partial x^3} = 0 \tag{17}$$

The first three of these conditions are obtained from Eqs. (2), (3), and (4) together with the definition of the thermal layer. The last two conditions are derived from the differential equation of heat conduction (Eq. 1). Applying Eqs. 13-17, the temperature profile takes the form

$$\frac{T-T_i}{F\delta/k} = \frac{1}{2} - \left(\frac{x}{\delta}\right) + \frac{3}{2}\left(\frac{x}{\delta}\right)^2 - \left(\frac{x}{\delta}\right)^3 + \frac{1}{4}\left(\frac{x}{\delta}\right)^4 \tag{18}$$

Substituting into Eq. (11), it is seen that

$$\theta = T_i\delta + \frac{F\delta^2}{20k} \tag{19}$$

Introducing Eqs. (2) and (19) into the heat-balance integral, Eq. (10), gives the following ordinary differential equation for δ:

$$\frac{1}{20}\frac{d\delta^2}{dt} = \alpha \tag{20}$$

By virtue of the initial condition, $\delta(0) = 0$,

$$\delta = \sqrt{20}\,\alpha t \tag{21}$$

The surface temperature is obtained by setting x=0 in Eq. (18) and applying Eq. (21). The result is:

$$T(0,t) = T_i + \frac{F}{k}\sqrt{(5/4)\alpha t} \tag{22}$$

The exact solution of this problem is given in Carslaw and Jaeger (33) and may be written as:

$$T(0,t) = T_i + \frac{F}{k}\sqrt{(4/\pi)\alpha t} \tag{23}$$

Since $\sqrt{4/\pi} = 1.13$ and $\sqrt{5/4} = 1.12$, the error is about 0.88% which compares with an error of about 9% for the P 2-method. Thus the P 4-method represents a significant improvement over the P 2-method.

The heating process represented by the fixed boundary problem will continue until the surface temperature reaches the equilibrium temperature T_s at which time $t=t_{sd}$; the start of dissociation. From Eqs. (21) and (23) we find

$$t_{sd} = \frac{4\,k^2(T_s-T_i)^2}{5\alpha F^2} \tag{24}$$

$$\delta = 4k\,(T_s-T_i)/F \qquad \text{at } T=t_{sd} \tag{25}$$

Substituting these equations into Eq. (18) gives the initial temperature profile, f(x), for the moving-boundary problem. With representative parameter values Eq. (25)

yields a small (~1 sec) value of t_{sd}, which justifies neglecting the time required to heat to dissociation.

Next apply the P 4-method to the solution of the moving-boundary problem described by Eqs. (5) Through (9). The heat-balance integral is obtained by integrating Eq. (5) over the thermal layer from x=X(t) to x=δ(t). After applying (7), one obtains

$$\frac{d}{dt}\theta - T_i\delta + \left(T_s + \frac{\rho\lambda\alpha}{k}\right)X = \frac{\alpha F}{k} \tag{26}$$

where

$$\theta = \int_{X(t)}^{\delta(t)} T\, dx \tag{27}$$

Once again, the temperature distribution is represented by a fourth-degree polynomial which satisfies the following five conditions:

$$T(X,t) = T_s \tag{28}$$

$$T(\delta,t) = T_i \tag{29}$$

$$\frac{\partial T(\delta,t)}{\partial x} = 0 \tag{30}$$

$$\frac{\partial^2 T(\delta,t)}{\partial x^2} = 0 \tag{31}$$

$$\frac{\partial^3 T(\delta,t)}{\partial x^3} = 0 \tag{32}$$

The first three of these conditions are obtained from Eqs.

(6) and (8) together with the definition of the thermal layer. The last two conditions are derived from the differential equation of heat conduction. Applying these conditions, one obtains the following distribution

$$\frac{T-T_s}{T_i-T_s} = 4\left(\frac{x-X}{\delta-X}\right) - 6\left(\frac{x-X}{\delta-X}\right)^2 + 4\left(\frac{x-X}{\delta-X}\right)^3 - \left(\frac{x-X}{\delta-X}\right)^4 \qquad (33)$$

Upon substituting Eq. (33) into Eq. (27), and applying the result in Eq. (26), one obtains

$$\frac{d\ (\delta-X)}{dt} + 5\ (1+\nu)\frac{dX}{dt} = \frac{5\alpha F}{k(T_s-T_i)} \qquad (34)$$

where

$$\nu = \frac{\rho\lambda\alpha}{k(T_s-T_i)} = \frac{\lambda}{C_p(T_s-T_i)} \qquad (35)$$

The dimensionless quantity ν is the ratio of the latent to sensible heat and is commonly known as the Stefan number.

Equation (34) involves the two unknowns $\delta-X$ and X, and consequently an additonal relationship between δ and X is required. This relationship can be obtained from the condition at the dissociation interface X(t). Upon substituting Eq. (33) into Eq.(7) one obtains

$$\rho\lambda\frac{dX}{dt} = F - \frac{4k(T_s-T_i)}{\delta-X} \qquad (36)$$

Equations (34) and (36) are two simultaneous differential equations for $(\delta-X)$ and X. The initial conditions are

$$X = 0 \qquad \text{at } t = t_{sd} \tag{37}$$

$$\delta = 4k(T_s - T_i)/F \qquad \text{at } t = t_{sd} \tag{38}$$

where t_{sd} is given by Eq. (24).

Elimination of dX/dt between Eqs. (34) and (36) gives the following differential equation:

$$\frac{d\zeta}{d\tau} - (1+\nu)\frac{1}{\zeta} + 1 = 0 \tag{39}$$

where

$$\zeta = \frac{F(\delta - X)}{4k(T_s - T_i)} \tag{40}$$

and

$$\tau = \frac{5\ F^2 t}{4\rho\lambda k(T_s - T_i)} \tag{41}$$

in terms of these dimensionless variables, the initial conditions, Eqs. (37) and (38), become

$$\zeta = 1 \qquad \text{at } \tau = \tau_{sd} \tag{42}$$

where τ_{sd} is the dimensionless start of dissociation time. Using Eqs. (24) and (41) one finds

$$\tau_{sd} = \frac{1}{\nu} \tag{43}$$

The solution of the differential equation, Eq. (39), subject to the initial condition, Eq. (42), is

$$\tau - \tau_{sd} = (1-\zeta) + (1+\nu)\ln\left(\frac{\nu}{(1+\nu)-\zeta}\right) \tag{44}$$

Next one obtains a differential equation for the rate of advance of the dissociation interface by rewriting Eq. (36) as

$$\frac{dX^*}{d\tau} = \frac{\zeta-1}{\zeta} \tag{45}$$

with the initial condition

$$X^* = 0 \qquad \text{at } \tau = 0 \tag{46}$$

where X^* is the dimensionless position of the moving front defined as

$$X^* = \frac{5\ FX}{4k(T_s-T_i)} \tag{47}$$

Elimination of $d\tau$ between Eqs. (39) and (45) gives the following differential equation:

$$\frac{dX^*}{d\zeta} = \frac{\zeta-1}{(1+\nu)-\zeta} \tag{48}$$

with

$$X^* = 0 \qquad \text{at } \zeta = 1 \tag{49}$$

The solution of this equation is given by

$$X^* = (1-\zeta) + \nu\ \text{ln}\left(\frac{\nu}{(1+\nu)-\zeta}\right) \tag{50}$$

Equations (44) and (50) give the position of the dissociation front X^* as a function of time τ. These are plotted in Figures 15 and 16 for various values of the Stefan number ν. Results from these figures can,

Figure 15

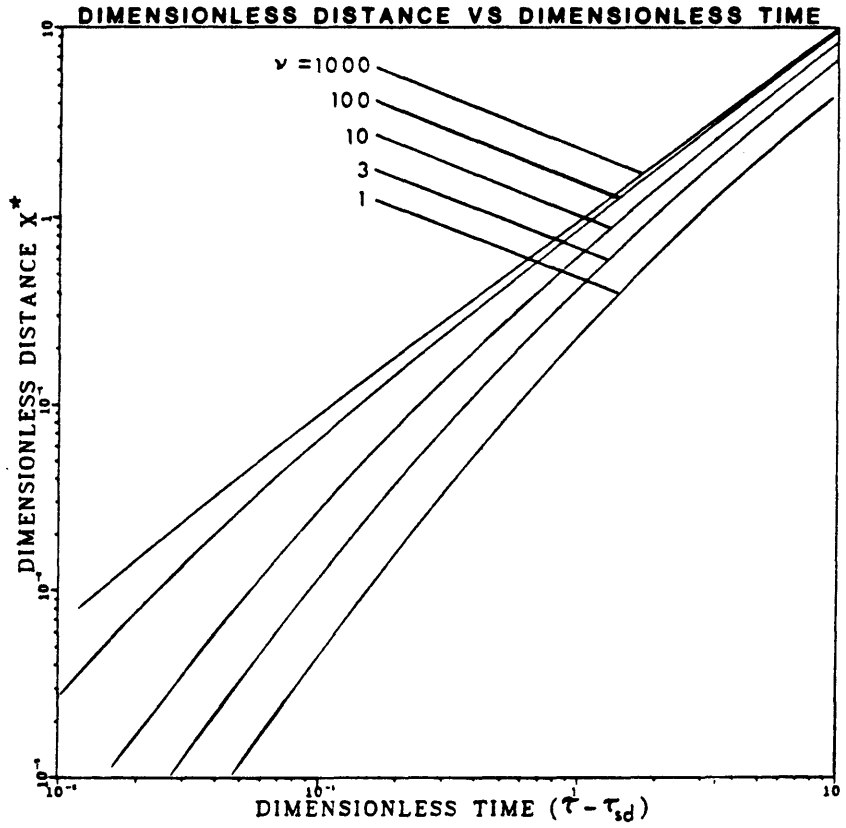
DIMENSIONLESS DISTANCE VS DIMENSIONLESS TIME
ν =1000
100
10
3
1
DIMENSIONLESS DISTANCE X*
DIMENSIONLESS TIME (τ - τsd)
10
1
10⁻¹
10⁻²
10⁻³
10⁻¹
10⁰
10¹

Figure 16

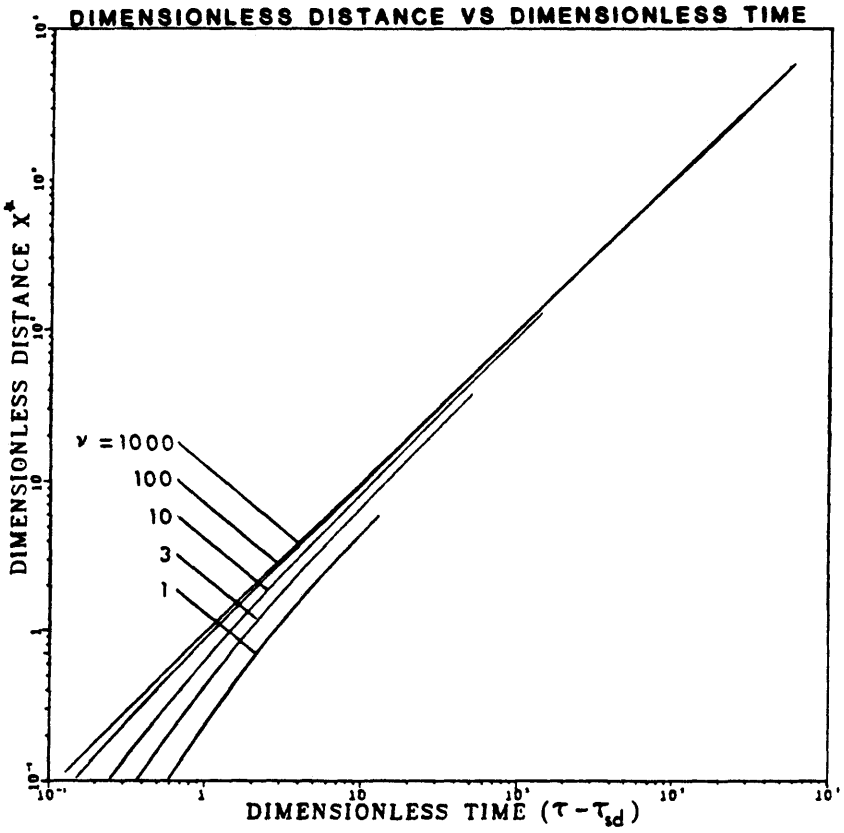
DIMENSIONLESS DISTANCE VS DIMENSIONLESS TIME
DIMENSIONLESS DISTANCE X*
DIMENSIONLESS TIME (τ - τsd)
ν = 1000
100
10
3
1

therefore, be used directly to determine the amount of hydrate dissociated as a function of time. One may also notice from these figures that the speed of the interface decreases with time; eventually attaining a constant value. Thus a long-time solution can be obtained by setting dX/dt equal to a constant in Eq. (36). It follows that $\zeta - X$ is constant and from Eq. (34) it is seen that

$$\frac{dX}{dt} = \frac{\alpha F/k(T_s - T_i)}{1+\nu} \qquad \text{for large } t \qquad (51)$$

This may be integrated to give the following long-time solution:

$$X^* = \frac{\nu}{1+\nu}(\tau - \tau_{sd}) \qquad (52)$$

This result is useful for practical calculations at large times.

One may determine the fraction of the incident flux which is used for dissociation and that fraction which is conducted into the sample. To determine these fractions consider the condition at the boundary, Eq. (7). This equation can be broken into two portions, the energy used for dissociation and the energy used in conduction, Eqs. (53) and (54).

$$f_D = \frac{\rho\lambda(dX/dt)}{F} \qquad (53)$$

$$f_C = \frac{-k(\partial T/\partial x)_X}{F} \tag{54}$$

By applying Eqs. (36) and (40) and the derivative of Eq. (18) at x = X, f_D and f_C become:

$$f_D = 1 - (1/\zeta) \tag{55}$$

$$f_C = 1 / \zeta \tag{56}$$

where ζ varies with time according to Eq. (44).

By applying the definition of dX/dt in Eq. (50) expressions for f_D and f_C may be determined for large times.

$$f_D = 1 - (1/\zeta) \tag{57}$$

$$f_c = 1/\zeta \tag{58}$$

where

$$\zeta = 1 + \nu \tag{59}$$

Eqs. (57) and (58) can be reexpressed in terms of the Stefan number.

$$f_D = \nu / (1+\nu) \tag{60}$$

$$f_C = 1 / (1+\nu) \tag{61}$$

Thus, as the value of the Stefan number increases the portion of the incident radiation used in dissociation also increases, while the portion used in conduction decreases. As an example consider the case when ν = 25. The fraction of the incident energy used to dissociate is 96.0%, while

4% is lost to conduction.

Appendix B

Physical Data

Ice

density(43)	0.913	gm/cm^3
heat capacity(43)	1.926	W.s/gm/K
thermal conductivity(44)	2.215	W/m/K
heat of sublimation(43)	2837.5	W.s/gm

Carbon Dioxide

density(45)	1.565	gm/cm^3
heat capacity(46)	1.243	W.s/gm/K
thermal conductivity(47)	0.200	W/m/K
heat of sublimation(45)	572.8	W.s/gm

Methane hydrate

density(1)	0.892	gm/cm^3
heat capacity(29)	2.010	W.s/gm/K
thermal conductivity(21)	0.393	W/m/K
heat of sublimation(48) (see calculation)	2618.8	W.s/gm

Heat of Dissociation Calculation for Methane Hydrate

The heat of dissociation of methane hydrates involves supplying enough energy to completely vaporize the hydrate. Since enthaply is a state function, a two step path is used to calculate the heat of dissociation. The first step involves supplying heat to change the hydrate into methane gas and ice. The second step is calculating the energy of sublimation of the ice. The heat of dissociation is the sum. This calculation was made for equilibrium hydrates at the formation conditions. These hydrates have a stoichiometric ratio of 1 gas molecule to 6.15 water molecules or 93.5% hydrate by mass.

The change in enthalpy of step one was calculated to be 140.3 W.s/gm using the vapor-ice-hydrate equilibrium data of Falabella and Vanpee (48). The enthalpy of step two is 2478.5 W.s/gm. Therefore, the calculated heat of dissociation is 2618.8 W.s/gm. The development of the Clayepron equation is shown below.

Derivation of Claypeyron equation.

The thermodynamic derivation begins with the Gibbs

Free Energy in the vapor phase equal to that in the liquid phase.

$$G^v = G^l$$

Using the definition of the Gibbs Free Energy and rearanging one obtains:

$$H^v - TS^v = H^l - TS^l$$

$$(H^v - H^l) = T(S^v - S^l)$$

The change in the Gibbs Free Energy is also equal in both phases.

$$dG^v = dG^l$$

Using the differential of the definition of the Gibbs Free Energy and the equation for ΔH from above one obtains.

$$dG = -SdT + VdP$$

$$-S^v dT + V^v dP = -S^l dT + V^l dP$$

$$-(S^v - S^l)dT = -(V^v - V^l)dP$$

$$\Delta S^{vap} = (V^v - V^l)dP$$

$$\Delta H^{vap} = T(V^v - V^l)\, dP/dT$$

Assume that $V^l << V^v$ and that the volume of the vapor is given by:

$$V^v = ZRT/P$$

Substitution of these assumptions and rearangement results in the Clayepron equation.

$$\Delta H^{vap} = ZR\ (dP/P)/(dT/T^2)$$

$$\Delta H^{vap} = -ZR\ (d\ln P)/(d(1/T))$$

Absorptivity Calculation

The procedure used to calculate the absorptivity is outlined below.

1. Determine the surface temperature of the radiant heater using the thermocouple.

2. Calculate the wavelength of greatest intensity of the emmitted radiation using Wiens' Law.

3. Locate data for the extinction coeefficient as a function of wavelength and use the value for the wavelength calculated in step 2.

4. Calculate the reflectivity using the Fresnel equation (49) for normally incident radiation in air.

5. Assume that the transmissivity is zero (based on examination of an absorbance versus thickness chart (48)) and calculate the absorptivity using the definition that the sum of the transmissivity, the absorptivity, and the reflectivity is equal to one.

Appendix C

Bomb Calorimetry Data

In Situ Hydrate Samples

The following data was taken while investigating the gas hydrates recovered from site 570 of the Deep Sea Drilling Project. The data taken during the calibration of the calorimeter and the testing of this calibraton using two unknowns is also included.

Calibration Run 1

Mass of deionized water	2000.0gm
Pellet mass	0.3955gm
Length of fuse wire	11.5cm
Length of uncombusted fuse wire	5.6cm
Pressure	28.0atm

Temperature Measurements	Time(secs)	Temp(^{o}C)
Preperiod	0	25.474
	60	25.474
	120	25.469
	180	25.469
	240	25.469
	300	25.469
Temperature Rise	345	25.80
	360	25.96
	375	25.10
	390	26.19
	405	26.26
	420	26.32
	480	26.42
	540	26.47
	600	26.48
	660	26.485
	720	26.485
	780	26.485
	840	26.485
	900	26.485

Calibration Run 2

Mass of deionized water	2000.0gm
Pellet mass	0.4694gm
Length of fuse wire	11.8cm
Length of uncombusted fuse wire	3.6cm
Pressure	28.75atm

Temperature Measurements	Time(secs)	Temp(^{o}C)
Preperiod	0	25.469
	60	25.469
	120	25.469
	180	25.469
	240	25.469
	300	25.469
Temperature Rise	345	25.85
	360	26.08
	375	26.18
	390	26.34
	405	26.42
	420	26.46
	480	26.615
	540	26.654
	600	26.675
	660	26.685
	720	26.690
	780	26.690
	840	26.690
	900	26.690

Calibration Run 3

Mass of deionized water	2000.0gm
Pellet mass	0.4486gm
Length of fuse wire	10.9cm
Length of uncombusted fuse wire	5.9cm
Pressure	28.5atm

Temperature Measurements	Time(secs)	Temp(^{o}C)
Preperiod	0	25.554
	60	25.554
	120	25.554
	180	25.554
	240	25.554
	300	25.554
Temperature Rise	345	25.91
	360	26.09
	375	26.27
	390	26.37
	405	26.45
	420	26.52
	480	26.644
	540	26.694
	600	26.709
	660	26.719
	720	26.719
	780	26.719
	840	26.719
	900	26.719

Calibration Run 4

Mass of deionized water	2000.0gm
Pellet mass	0.5621gm
Length of fuse wire	11.9cm
Length of uncombusted fuse wire	5.0cm
Pressure	27.0atm

Temperature Measurements	Time(secs)	Temp(^{o}C)
Preperiod	0	22.894
	60	22.894
	120	22.894
	180	22.894
	240	22.894
	300	22.894
Temperature Rise	345	23.35
	360	23.61
	375	23.77
	390	23.90
	405	24.00
	420	24.10
	480	24.267
	540	24.325
	600	24.349
	660	24.367
	720	24.367
	780	24.367
	840	24.367

Calibration Run 5

Mass of deionized water	2000.0gm
Pellet mass	0.5413gm
Length of fuse wire	11.0cm
Length of uncombusted fuse wire	7.8cm
Pressure	28.0atm

Temperature Measurements	Time(secs)	Temp(^{o}C)
Preperiod	0	23.007
	60	23.009
	120	23.009
	180	23.009
	240	23.009
	300	23.009
Temperature Rise	345	23.45
	360	23.69
	375	23.86
	390	23.99
	405	24.07
	420	24.15
	480	24.284
	540	24.379
	600	24.399
	660	24.404
	720	24.409
	780	24.409
	840	24.409
	900	24.409

Unknown Test (camphor)

Mass of deionized water	2000.0gm
Pellet mass	0.5083gm
Length of fuse wire	11.9cm
Length of uncombusted fuse wire	4.2cm
Pressure	28.0atm

Temperature Measurements	Time(secs)	Temp($^{o}_{C}$)
Preperiod	0	25.379
	60	25.379
	120	25.379
	180	25.379
	240	25.379
	300	25.379
Temperature Rise	345	26.03
	360	26.33
	375	26.57
	390	26.73
	405	26.88
	420	26.99
	480	27.196
	540	27.276
	600	27.301
	660	27.306
	720	27.311
	780	27.316
	840	27.316
	900	27.316

Unknown Test (phenol)

Mass of deionized water	2000.0gm
Pellet mass	0.6028gm
Length of fuse wire	12.8cm
Length of uncombusted fuse wire	9.3cm
Pressure	28.5atm

Temperature Measurements	Time(secs)	Temp(^{o}C)
Preperiod	0	25.379
	60	25.379
	120	25.379
	180	25.379
	240	25.379
	300	25.379
Temperature Rise	345	26.03
	360	26.33
	375	26.58
	390	26.74
	405	26.88
	420	27.00
	480	27.196
	540	27.276
	600	27.301
	660	27.306
	720	27.311
	780	27.316
	840	27.316
	900	27.316

Hydrate Sample Run 1

Mass of deionized water		2000.0gm
Mass of sample		8.729gm
Length of fuse wire		11.1cm
Length of uncombusted fuse wire		-----
Pressure		27.5atm
Temperature Measurements	Time(secs)	Temp(^{0}C)
Preperiod	0	23.662
	60	23.662
	120	23.662
	180	23.662
	240	23.662
	300	23.662
Temperature Rise	Sample did not ignite	
Mass of Sedimnt		0.092gm

Hydrate Sample Run 2

Mass of deionized water		2000.0gm
Mass of sample		2.960gm
Length of fuse wire		9.4cm
Length of uncombusted fuse wire		5.9cm
Pressure		28.0atm
Temperature Measurements	Time(secs)	Temp(^{o}C)
Preperiod	0	24.667
	60	24.667
	120	24.667
	180	24.667
	240	24.667
	300	24.667
Temperature Rise	Sample did not ignite	
Mass of sediment		0.027gm

Hydrate Sample Run 3

Mass of deionized water		2000.0gm
Sample mass		3.802gm
Length of fuse wire		10.1cm
Length of uncombusted fuse wire		4.2cm
Pressure		10.5atm

Temperature Measurements	Time(secs)	Temp($^{o}_{C}$)
Preperiod	0	25.109
	60	25.109
	120	25.109
	180	25.109
	240	25.109
	300	25.109
Temperature Rise	345	25.40
	360	25.47
	375	25.55
	390	25.59
	405	25.62
	420	25.67
	480	25.709
	540	25.729
	600	25.739
	660	25.744
	720	25.749
	780	25.774
	840	25.774
	900	25.774
	960	25.774

Mass of sediment	0.100gm

Hydrate Sample Run 4

Mass of deionized water		2000.0gm
Mass of sample		4.784gm
Length of fuse wire		12.4cm
Length of uncombusted fuse wire		-----
Pressure		10atm
Temperature Measurements	Time(secs)	Temp(^{o}C)
Preperiod	0	22.747
	60	22.747
	120	22.747
	180	22.747
	240	22.747
	300	22.747
Temperature Rise	Sample did not ignite	
Mass of sediment		0.211gm

Hydrate Sample Run 5

Mass of deionized water		2000.0gm
Mass of sample		1.588gm
Length of fuse wire		10.7cm
Length of uncombusted fuse wire		5.7cm
Pressure		2.2atm

Temperature Measurements	Time(secs)	Temp($^{o}_{-}$C)
Preperiod	0	25.449
	60	25.449
	120	25.449
	180	25.449
	240	25.449
	300	25.449
Temperature Rise	345	25.52
	360	25.55
	375	25.58
	390	25.59
	405	25.60
	420	25.61
	480	25.634
	540	25.639
	600	25.644
	660	25.649
	720	25.649
	780	25.649
	840	25.649
	900	25.649

Mass of sediment	0.105gm

Hydrate Sample Run 6

Mass of deionized water		2000.0gm
Mass of sample		2.94gm
Length of fuse wire		10.8cm
Length of uncombusted fuse wire		-----
Pressure		6.0atm
Temperature Measurements	Time(secs)	Temp(^{o}C)
Preperiod	0	25.679
	60	25.679
	120	25.679
	180	25.679
	240	25.679
	300	25.679
Temperature Rise	Sample did not ignite	
Mass of sediment		0.060gm

Hydrate Sample Run 7

Mass of deionized water		2000.0gm
Mass of sample		2.135gm
Length of fuse wire		10.6cm
Length of uncombusted fuse wire		5.1cm
Pressure		1atm

Temperature Measurements	Time(secs)	Temp($^{o}_{C}$)
Preperiod	0	25.699
	60	25.699
	120	25.699
	180	25.699
	240	25.694
	300	25.694
Temperature Rise	345	25.70
	360	25.71
	375	25.73
	390	25.73
	405	25.739
	420	25.744
	480	25.744
	540	25.744
	600	25.744

Mass of sediment	0.078gm

Hydrate Sample Run 8

Mass of deionized water		2000.0gm
Mass of sample		1.814gm
Length of fuse wire		10.7cm
Length of uncmobusted fuse wire		-----
Pressure		1.0atm
Temperature Measurements	Time(secs)	Temp(^{o}C)
Preperiod	0	23.834
	60	23.834
	120	23.834
	180	23.834
	240	23.834
	300	23.834
Temperature Rise	Sample did not ignite	
Mass of sediment		0.102gm

Hydrate Sample Run 9

Mass of deionized water		2000.0gm
Mass of sample		4.169gm
Length of fuse wire		11.0cm
Length of uncombusted fuse wire		-----
Pressure		1.0atm
Temperature Measurements	Time(secs)	Temp(^{o}C)
Preperiod	0	23.372
	60	23.372
	120	23.372
	180	23.372
	240	23.372
	300	23.372
Temperature Rise	Sample did not ignite	
Mass of sediment		1.590gm

Hydrate Sample Run 10

Mass of deionized water		2000.0gm
Mass of sample		9.274gm
Length of fuse wire		11.2cm
Length of uncombusted fuse wire		------
Pressure		1.0atm
Temperature Measurements	Time(secs)	Temp(^{o}C)
Preperiod	0	25.774
	60	25.774
	120	25.774
	180	25.774
	240	25.769
	300	25.769
Temperature Rise	Sample did not ignite	
Mass of sediment		5.696gm

Appendix D

Bomb Calorimetry Data

Laboratory Methane Hydrates

The following data was taken while determining the usefulness of the laboratory prepared methane hydrates. The data taken during the calibration of the calorimeter and the testing of this calibration using two unknowns is also included.

Calibration Run 1

Mass of deionized water	2000.0gm
Pellet mass	0.4584gm
Length of fuse wire	10.4cm
Length of uncombusted fuse wire	5.1cm
Pressure	26.5atm

Temperature Measurements	Time(secs)	Temp(^{o}C)
Preperiod	0	24.490
	60	24.490
	120	24.490
	180	24.485
	240	24.485
	300	24.485
Temperature Rise	345	24.88
	360	25.04
	375	25.20
	390	25.30
	405	25.38
	420	25.44
	480	25.565
	540	25.615
	600	25.630
	660	25.640
	720	25.640
	780	25.640
	840	25.640
	900	25.640

Calibration Run 2

Mass of deionized water	2000.0gm
Pellet mass	0.5670gm
Length of fuse wire	11.1cm
Length of uncombusted fuse wire	4.2cm
Pressure	26.5atm

Temperatue Measurements	Time(secs)	Temp($^{o}_{C}$)
Preperiod	0	24.270
	60	24.270
	120	24.265
	180	24.265
	240	24.620
	300	24.260
Temperature Rise	345	24.74
	360	24.98
	375	25.16
	390	25.30
	405	25.38
	420	25.46
	480	25.610
	540	25.665
	600	25.695
	660	25.700
	720	25.700
	780	25.700
	840	25.700
	900	25.700

Calibration Run 3

Mass of deionized water	2000.0gm
Pellet mass	0.6287gm
Length of fuse wire	11.4cm
Length of uncombusted fuse wire	5.7cm
Pressure	26.3atm

Temperature Measurements	Time(secs)	Temp(^{o}C)
Preperiod	0	24.130
	60	24.130
	120	24.130
	180	24.125
	240	24.125
	300	24.125
Temperature Rise	345	24.60
	360	24.94
	375	25.09
	390	25.28
	405	25.38
	420	25.45
	480	25.635
	540	25.700
	600	25.715
	660	25.725
	720	25.725
	780	25.725
	840	25.725
	900	25.725

Calibration Run 4

Mass of deionized water	2000.0gm
Pellet mass	0.5480gm
Length of fuse wire	11.6cm
Length of uncombusted fuse wire	4.3cm
Pressure	25.5atm

Temperature Measurements	Time(secs)	Temp($^{o}_{C}$)
Preperiod	0	24.045
	60	24.045
	120	24.045
	180	24.045
	240	24.045
	300	24.045
Temperature Rise	345	24.48
	360	24.72
	375	24.90
	390	25.02
	405	25.12
	420	25.20
	480	25.360
	540	25.405
	600	25.535
	660	25.440
	720	25.440
	780	25.440
	840	25.440
	900	25.440

Calibration Run 5

Mass of deionized water	2000.0gm
Pellet mass	0.6187gm
Length of fuse wire	11.9cm
Length of uncombusted fuse wire	6.5cm
Pressure	26.0atm

Temperature Measurements	Time(secs)	Temp(^{o}C)
Preperiod	0	24.515
	60	24.515
	120	24.515
	180	24.515
	240	24.515
	300	24.515
Temperature Rise	345	25.04
	360	25.28
	375	25.50
	390	25.64
	405	25.73
	420	25.82
	480	26.000
	540	26.055
	600	26.075
	660	26.080
	720	26.085
	780	26.085
	840	26.085
	900	26.085

Unknown Test (naphthalene)

Mass of deionized water	2000.0gm
Pellet mass	0.7900gm
Length of fuse wire	11.4cm
Length of uncombusted fuse wire	5.5cm
Pressure	26.0atm

Temperature Measurements	Time(secs)	Temp(^{o}C)
Preperiod	0	24.625
	60	24.625
	120	24.625
	180	24.625
	240	24.625
	300	24.625
Temperature Rise	345	25.40
	360	26.00
	375	26.44
	390	26.72
	405	27.00
	420	27.18
	480	27.555
	540	27.670
	600	27.715
	660	27.730
	720	27.735
	780	27.735
	840	27.735
	900	27.735

Unknown Test (benzoic acid)

Mass of deionized water	2000.0gm
Pellet mass	0.8027gm
Length of fuse wire	12.6cm
Length of uncombusted fuse wire	5.9cm
Pressure	26.0atm

Temperature Measurements	Time(sec)	Temp(^{o}C)
Preperiod	0	25.405
	60	25.405
	120	25.405
	180	25.405
	240	25.405
	300	25.405
Temperature Rise	345	26.20
	360	26.56
	375	26.80
	390	26.98
	405	27.12
	420	27.20
	480	27.405
	540	27.470
	600	27.500
	660	27.500
	720	27.500
	780	27.500
	840	27.500
	900	27.500

Hydrate Sample Run 1

Mass of deionized water	2000.0gm
Mass of sample	1.156gm
Length of fuse wire	12.5cm
Length of uncombusted fuse wire	6.2cm
Pressure	1.0atm

Temperature Measurements	Time(secs)	Temp(^{o}C)
Preperiod	0	23.650
	60	23.650
	120	23.650
	180	23.650
	240	23.650
	300	23.650
Temperature Rise	345	23.80
	360	23.83
	375	23.85
	390	23.87
	405	23.88
	420	23.90
	480	23.915
	540	23.930
	600	23.935
	660	23.940
	720	23.940
	780	23.940
	840	23.940
	900	23.940

Hydrate Sample Run 2

Mass of deionized water	2000.0gm
Mass of sample	1.125gm
Length of fuse wire	10.7cm
Length of uncombusted fuse wire	6.3cm
Pressure	2.4atm

Temperature Measurements	Time(secs)	Temp(^{o}C)
Preperiod	0	24.415
	60	24.415
	120	24.415
	180	24.415
	240	24.415
	300	24.415
Temperature Rise	345	24.68
	360	24.76
	375	24.80
	390	24.83
	405	24.86
	420	24.88
	480	24.920
	540	24.935
	600	24.945
	660	24.950
	720	24.955
	780	24.555
	840	24.555
	900	24.555

Hydrate Sample Run 3

Mass of deionized water	2000.0gm
Mass of sample	1.217gm
Length of fuse wire	13.8cm
Length of uncombusted fuse wire	7.9cm
Pressure	1.0atm

Temperature Measurements	Time(secs)	Temp(^{o}C)
Preperiod	0	24.025
	60	24.025
	120	24.025
	180	24.025
	240	24.025
	300	24.025
Temperature Rise	345	24.17
	360	24.21
	375	24.23
	390	24.25
	405	24.26
	420	24.27
	480	24.200
	540	24.315
	600	24.320
	660	24.325
	720	24.330
	780	24.330
	840	24.330
	900	24.330

Appendix E

Dissociation Data

The following data was taken using the dissociation apparatus. The data for the ice experiments which were used to calibrate and check the system are presented first. The data used in the solid carbon dioxide experiments is also included. The data for the three experiments on the laboratory prepared methane hydrates follows the other data.

Ice Experiment 1

Length of ice cylinder 2.125in

Radius of ice cylinder 0.196in

Dissociation Data

Time(min)	Mass Loss(gm)
0	0.000
1	0.036
2	0.072
3	0.110
4	0.145
5	0.183
6	0.220
7	0.256
8	0.292
9	0.328
10	0.364
11	0.399
12	0.435
13	0.470
14	0.503
15	0.539
16	0.573
17	0.608
18	0.634

Ice Experiment 2

Length of ice cylinder 2.125in

Radius of ice cylinder 0.196in

Dissociation Data

Time(min)	Mass Loss(gm)
0	0.000
1	0.026
2	0.063
3	0.100
4	0.135
5	0.170
6	0.195
7	0.238
8	0.270
9	0.302
10	0.335
11	0.369
12	0.402
13	0.435
14	0.468
15	0.500
16	0.532
17	0.564
18	0.595
19	0.628
20	0.660
21	0.691
22	0.722
23	0.752
24	0.783
25	0.815
26	0.846
27	0.878
28	0.910

Ice Experiment 3

Length of ice cylinder 2.125in

Radius of ice cylinder 0.196in

Dissociation Data

Time(min)	Mass Loss(gm)
0	0.000
1	0.037
2	0.075
3	0.112
4	0.139
5	0.186
6	0.222
7	0.260
8	0.297
9	0.332
10	0.369
11	0.404
12	0.440
13	0.475
14	0.511
15	0.536
16	0.581
17	0.616
18	0.650
19	0.685
20	0.720
21	0.754
22	0.788
23	0.821
24	0.856
25	0.890
26	0.923
27	0.956

Ice Experiment 4

Length of ice cylinder 2.125in

Radius of ice cylinder 0.196in

Dissociation Data

Time(min)	Mass Loss(gm)
0	0.000
1	0.034
2	0.074
3	0.110
4	0.148
5	0.184
6	0.218
7	0.254
8	0.289
9	0.324
10	0.359
11	0.394
12	0.425
13	0.457
14	0.492
15	0.524
16	0.557

Ice Experiment 5

Length of ice cylinder 2.063in

Radius of ice cylinder 0.196in

Dissociation Data

Time(min)	Mass Loss(gm)
0	0.000
1	0.033
2	0.071
3	0.106
4	0.143
5	0.181
6	0.216
7	0.253
8	0.290
9	0.326
10	0.363
11	0.399
12	0.433
13	0.470
14	0.504
15	0.541
16	0.575
17	0.610
18	0.643
19	0.678
20	0.713
21	0.746
22	0.780
23	0.813
24	0.846
25	0.880
26	0.913
27	0.945

Carbon Dioxide Data

Run Number	dM/dt (gm)	Radius (in)	Length (in)	Mass loss at dm/dt(gm)
1	0.180	0.203	2.000	1.000
2	0.174	0.204	2.000	0.750
3	0.136	0.172	1.933	0.350
4	0.154	0.185	1.875	0.600
5	0.165	0.192	2.000	1.000
6	0.171	0.192	2.000	1.000
7	0.139	0.170	2.000	0.600
8	.174	0.208	2.000	1.000

Methane Hydrate Experiment 1

Length of hydrate sample 1.950in

Radius of hydrate sample 0.206in

Calculated density 46.966lb/ft^3

Dissociation data

Time(min)	Mass Loss(gm
0	0.000
1	0.042
2	0.083
3	0.121
4	0.160
5	0.200
6	0.238
7	0.275
9	0.312
10	0.352
11	0.390
12	0.429
13	0.466
14	0.504
15	0.578
16	0.615
17	0.651
18	0.690
19	0.727
20	0.760

Methane Hydrate Experiment 2

Length of hydrate sample 1.980in

Radius of hydrate sample 0.206in

Calculated density 51.72lb/ft^3

Dissociation data

Time(min)	Mass Loss(gm)
0	0.000
1	0.036
2	0.077
3	0.119
4	0.161
5	0.205
6	0.249
7	0.290
8	0.334
9	0.379
10	0.421
11	0.462
12	0.504
13	0.544
14	0.585
15	0.627
16	0.666
17	0.707
18	0.745
19	0.785
20	0.825

Methane Hydrate Experiment 3

Length of hydrate sample 1.700in

Radius of hydrate sample 0.206in

Calculate density 43.989lb/ft^3

Dissociation data

Time(min)	Mass Loss(gm)
0	0.000
1	0.038
2	0.076
3	0.113
4	0.150
5	0.186
6	0.220
7	0.253
8	0.288
9	0.320
10	0.352
11	0.384
12	0.416
13	0.448
14	0.480
15	0.512
16	0.542
17	0.574